COUPLING OF SURFACE AND INTERNAL GRAVITY WAVES: A HAMILTONIAN MODEL

Kenneth M. Watson, et al

Physical Dynamics, Incorporated

Prepared for:

Defense Advanced Research Projects Agency
Rome Air Development Center

April 1974

RADC-TR-74-129
Technical Report
April 1974

COUPLING OF SURFACE AND INTERNAL GRAVITY WAVES: A HAMILTONIAN MODEL

Physical Dynamics Inc.

Sponsored By
Defense Advanced Research Projects Agency
ARPA Order No. 1649

Approved for public release;
distribution unlimited.

The views and conclusions contained in this document are those of the authors and should not be interpreted as necessarily representing the official policies, either expressed or implied, of the Defense Advanced Research Projects Agency or the U. S. Government.

Rome Air Development Center
Air Force Systems Command
Griffiss Air Force Base, New York 13441

Unclassified

SECURITY CLASSIFICATION OF THIS PAGE (When Data Entered)

REPORT DOCUMENTATION PAGE		READ INSTRUCTIONS BEFORE COMPLETING FORM
1 REPORT NUMBER RADC-TR-74-129	2 GOVT ACCESSION NO.	3. RECIPIENT'S CATALOG NUMBER AD-911 775
4 TITLE (and Subtitle) COUPLING OF SURFACE AND INTERNAL GRAVITY WAVES: A HAMILTONIAN MODEL		5 TYPE OF REPORT & PERIOD COVERED Scientific. Interim. 6. PERFORMING ORG. REPORT NUMBER PD-73-032
7 AUTHOR(s) Kenneth M. Watson Bruce J. West Bruce T. Cohen		8. CONTRACT OR GRANT NUMBER(s) F30602-72-C-0494
9. PERFORMING ORGANIZATION NAME AND ADDRESS Physical Dynamics, Inc. P.O. Box 1069 Berkeley, CA 94701		10. PROGRAM ELEMENT, PROJECT, TASK AREA & WORK UNIT NUMBERS Project No. 1649 Program Code No. 2E20 ARPA Order 1649
11. CONTROLLING OFFICE NAME AND ADDRESS Defense Advanced Research Projects Agency, 1400 Wilson Blvd, Arlington, VA 22209		12. REPORT DATE April 1974 13. NUMBER OF PAGES 88
14. MONITORING AGENCY NAME & ADDRESS(if different from Controlling Office) RADC/OSCE Griffiss AFB, New York 13441		15. SECURITY CLASS. (of this report) Unclassified 15a. DECLASSIFICATION/DOWNGRADING SCHEDULE

16. DISTRIBUTION STATEMENT (of this Report)

Approved for public release; distribution unlimited.

17 DISTRIBUTION STATEMENT (of the abstract entered in Block 20, if different from Report)

18 SUPPLEMENTARY NOTES

19. KEY WORDS (Continue on reverse side if necessary and identify by block number)

eigenmodes
Hamiltonian
internal wave dynamics
surface spectrum-internal wave spectrum interaction

20 ABSTRACT (Continue on reverse side if necessary and identify by block number)

The dynamics of the coupling of linear internal gravity waves and linear surface gravity waves on the ocean is studied using a Hamiltonian formalism and action-angle variables. The dynamic equations are solved both numerically and in some analytic approximations. The results compare favorably with the interaction experiments of Lewis, Lake and Ko the "resonant triad" experiments of Joyce and some satellite observations of Apel et al. The growth time for internal waves generated by the resonant interaction of

DD FORM 1 JAN 73 1473 EDITION OF 1 NOV 65 IS OBSOLETE

Unclassified

SECURITY CLASSIFICATION OF THIS PAGE (When Data Entered)

Unclassified

SECURITY CLASSIFICATION OF THIS PAGE(When Data Entered)

20.
Abstract

surface waves is calculated using the Garrett-Munk ocean model and the Phillips spectrum for surface waves. Energy exchange rates are deduced.

COUPLING OF SURFACE AND INTERNAL GRAVITY WAVES: A HAMILTONIAN MODEL

K. M. Watson
B. J. West
B. I. Cohen

Contractor: Physical Dynamics Inc.
Contract Number: F30602-72-C-0494
Effective Date of Contract: 1 May 1972
Contract Expiration Date: 31 December 1974
Amount of Contract: $319,925.00
Program Code Number: 4E20

Principal Investigator: J. Alex Thomson
Phone: 415 848-3063

Project Engineer: Leonard Strauss
Phone: 315 330-3055

This research was supported by the Defense Advanced Research Projects Agency of the Department of Defense and was monitored by Leonard Strauss (OCSE) Griffiss AFB NY 13441.

This report has been reviewed by the RADC Information Office (OI) and is releasable to the National Technical Information Service (NTIS). At NTIS it will be releasable to the general public, including foreign nations.

APPROVED: Leonard Strauss

LEONARD STRAUSS
Project Engineer

ABSTRACT

The dynamics of the coupling of linear internal gravity waves and linear surface gravity waves on the ocean is studied using a Hamiltonian formalism and action-angle variables. The dynamic equations are solved both numerically and in some analytic approximations. The results compare favorably with the interaction experiments of Lewis, Lake and Ko the "resonant triad" experiments of Joyce and some satellite observations of Apel et al. The growth time for internal waves generated by the resonant interaction of surface waves is calculated using the Garrett-Munk ocean model and the Phillips spectrum for surface waves. Energy exchange rates are deduced.

TABLE OF CONTENTS

Section		Page
	ABSTRACT	
I.	INTRODUCTION	1
II.	THE COUPLING OF SURFACE AND INTERNAL WAVES	6
III.	APPLICATIONS TO LABORATORY EXPERIMENTS	20
IV.	APPLICATIONS TO OCEAN WAVES	25
V.	GENERATION OF INTERNAL WAVES FROM A SATURATED SURFACE SPECTRUM	41
VI.	VISIBILITY OF INTERNAL WAVES ON OCEAN SURFACE	52
VII.	DISCUSSION AND CONCLUSIONS	64
	REFERENCES	66
	ACKNOWLEDGMENT	68
	APPENDIX	69

I. INTRODUCTION

The possible importance of surface waves for the generation of internal waves is mentioned by Phillips (1966) and models for this have been studied by Ball (1964), Thorpe (1966), and Kenyon (1968). Tank experiments to study the interaction of surface and internal waves have been reported by Lewis, Lake, and Ko (1974) and by Joyce (1974).

Synthesis of observations of internal waves in the deep ocean have been made by Garrett and Munk (1972a), (1975), who have proposed an explicit equilibrium spectrum for internal waves. Suggested sources of energy to drive internal waves are tidal currents, atmospheric pressure and stress fluctuations, and surface waves [see for example Phillips (1966), Chapter 5 or Thorpe (1975)]. The relative importance of these mechanisms at various internal wavenumbers is not presently known. If it is not saturated one might anticipate that energy is fed into the internal wave spectrum at longer and intermediate wavelengths and cascades by nonlinear interactions to the shortest internal wave wavelengths, where it is dissipated by wave breaking.

The purpose of this paper is to study the generation of internal waves by surface waves. We shall simplify the dynamics by treating the surface wave and internal wave motion in the linear approximation. The nonlinear coupling will be treated in the lowest non-vanishing order. To further simplify our analysis we shall assume (not unarbitrarily) that the wavenumbers and frequencies of the surface waves studied are large compared to the wavenumbers and frequencies of the internal waves of interest. The resulting dynamics will be expressed in Hamiltonian form and the Hamiltonian equations of motion expressed using action-angle variables. Both analytic approximations and numerical integration of these equations will be described.

For the purposes of this paper we shall model the ocean as follows. In the absence of wave motion the surface is assumed to locally coincide with the plane $z = 0$ of a rectangular coordinate system. The bottom is assumed to coincide with the plane $z = -H$. In order to use discrete Fourier expansions, a large rectangular ocean area A_o, with periodic boundary conditions, will be considered.

The density $\bar{\rho}(z)$ is assumed to have the following characteristics:

$\bar{\rho}(z) = \rho_o$, a constant, for $-D < z < 0$.

A thin thermocline with density change $\delta\rho$ occurs at $z = -D$. For $-H < z < -D$, $\bar{\rho}(z)$ is a monotonically decreasing function of z.

It is the Brunt-Väisälä frequency $N(z)$ which will appear in our equations for the internal waves [see, for example, Phillips (1966), Chapter 5]. The chosen model for the ocean implies that

$$N(z) = 0 \qquad , -D < z < 0,$$

$$N(z) = \left[-(g/\rho_o)\ \frac{d\bar{\rho}(z)}{dz}\right]^{1/2}, \quad -H < z < -D,$$

and

$$\int_{-D-\delta}^{-D+\delta} N^2(z)dz = g\ \delta\rho/\rho_o \quad , \tag{1}$$

where (2δ) is a small interval somewhat greater than the thickness of the thermocline. The quantity g represents the acceleration of gravity.

Although our dynamical equations will be obtained for this rather general model, the numerical calculations will be based on either of two more specific models. The first is that of Garrett and Munk (1972a):

$$N(z) = 0 \qquad , \qquad -D < z < 0,$$

$$N(z) = N_o \exp\left[(z + D)/b\right], \quad -H < z < -D,$$

$$N_o = 5.2 \times 10^{-3} \text{ sec}^{-1},$$

$$H = 5000 \text{ meters}$$

$$b = 1200 \text{ meters}. \qquad (2)$$

The internal wave eigenmodes for this model will be obtained and used in the WKB approximation.

The second model which we shall use is the somewhat unrealistic, but convenient, thin thermocline model:

$$N(z) = 0, \text{ except near } z = -D,$$

$$\int_{-D-\delta}^{-D+\delta} N^2(z)\,dz = g\,\delta\rho/\rho_o \quad . \qquad (3)$$

A constant Brunt-Väisälä frequency model is sometimes used. Kenyon (1968), for example, has studied the coupling of surface and internal waves using this model. We shall see that this model leads to very much weaker coupling than the Garrett-Munk model or the thin thermocline model [already observed by Joyce (1974)] and is presumably unrealistic for studying the generation of internal waves by surface waves.

The derivation of the equations for coupled surface and internal waves will be outlined in Section II. Applications to the tank experiments of Lewis et al. (1974) and Joyce (1974) will be described in Section III. Miscellaneous applications, including the generation of internal waves by a large amplitude swell [Apel et al. (1975a)], will be described in Section IV. The rate of generating internal waves by a

saturated spectrum of surface waves will be studied, including the dependence on mixed layer thickness D and thermocline strength $\delta\rho/\rho_o$ in Section V. The results of some numerical calculations of the development of a mottled appearance of the surface as the internal waves grow in amplitude [Apel, et al. (1975b)] will be shown in Section VI.

II. THE COUPLING OF SURFACE AND INTERNAL WAVES

The equations describing mutual coupling of surface and internal waves will be presented in this section. In the mixed layer, corresponding to $-D < z < 0$, the flow is treated as irrotational and the fluid velocity $\underset{\sim}{u}$ can be expressed as the gradient of a potential $\hat{\phi}(\underset{\sim}{r},z)$. [Here, and elsewhere in this paper we let $\underset{\sim}{r} = (x,y)$ represent a vector in the horizontal plane $z = 0$.]

We have assumed that the internal wave modes of interest to us have much lower characteristic frequencies and much longer wavelengths than have the surface waves. This suggests writing the velocity potential $\hat{\phi}$ in the form

$$\hat{\phi}(\underset{\sim}{r},z) = \phi(\underset{\sim}{r},z) + \Phi(\underset{\sim}{r},z) \quad . \tag{4}$$

Here ϕ contains the high frequency, high wavenumber components (surface waves) of $\hat{\phi}$ and Φ contains the low frequency, low wavenumber components (internal waves) of $\hat{\phi}$. Similarly, we can write the vertical displacement h, due to wave motion, of the ocean surface as a sum of a high frequency part ζ and a low frequency part H:

$$h(\underset{\sim}{r},t) = \zeta(\underset{\sim}{r},t) + H(\underset{\sim}{r},t) \quad . \tag{5}$$

Bernoulli's equation and the kinematic boundary condition on the surface $z = h(\underset{\sim}{r},t)$ are, respectively,

$$\frac{\partial \hat{\phi}}{\partial t} + \frac{1}{2} (\nabla \hat{\phi})^2 + gh = 0 \quad , \quad z = h \quad ,$$

$$\frac{\partial h}{\partial t} + (\nabla_s \hat{\phi}) \cdot (\nabla_s h) = \frac{\partial \hat{\phi}}{\partial z} \quad , \quad z = h \quad , \tag{6}$$

where ∇_s is the two-dimensional gradient operator, i.e.,

$$\nabla_s \equiv \left(\frac{\partial}{\partial x} , \frac{\partial}{\partial y} \right) .$$

For small amplitude waves the fluid motion below the ocean surface is described by the equation [see for example, Phillips (1966), Chapter 5]

$$\frac{\partial^2}{\partial t^2} \left(\frac{\partial}{\partial z^2} + \nabla_s^2 \right) w(\underset{\sim}{r},z,t) + N^2(z) \nabla_s^2 w(\underset{\sim}{r},z,t) = 0. \tag{7}$$

Here w is the vertical component of the fluid velocity and N is the Brunt-Väisälä frequency given by Eq. (1). We have assumed that $N = 0$ in the mixed layer, where $w = \frac{\partial \hat{\phi}}{\partial z}$. In the region of the thermocline and below, we assume that the flow w is associated with internal waves only.

Because we have supposed the wavelengths of the surface waves to be small compared to those of the internal waves, and also not significantly larger than the thickness D of the mixed layer, the nonlinear terms responsible for the coupling between the surface and internal waves are contained in the surface boundary conditions (6).

Near the surface, the low frequency fluid velocity associated with internal waves is

$$\bar{U}(\underset{\sim}{r},t) = \nabla\phi|_{z=0} \equiv \underset{\sim}{U}(\underset{\sim}{r},t) + \hat{\underset{\sim}{k}}\,\bar{U}_z(\underset{\sim}{r},t) \tag{8}$$

where $\underset{\sim}{U}$ and $\bar{U}_z$ are the horizontal and vertical currents, respectively. The corresponding high frequency velocity field associated with surface waves is

$$\underset{\sim}{v} = \nabla\phi \quad . \tag{9}$$

The properties of internal waves permit us to assume that

$$|\bar{U}_z| << |\underset{\sim}{U}| \quad ,$$

$$|H| << |\zeta| \quad ,$$

$$|\nabla_s^2(H)/H| << |\nabla_s^2(\zeta)/\zeta| \quad . \tag{10}$$

The first two inequalities describe the fact that for internal wave motion there is little displacement of the ocean surface. The third inequality states that the surface curvature due to internal waves is expected to be much less than that due to surface waves.

To describe the surface wave motion, we first define the high frequency velocity potential on the surface $z = H(\underset{\sim}{r},t)$

$$\phi_s(\underset{\sim}{r},t) \equiv \phi(\underset{\sim}{r},\ z = H(\underset{\sim}{r},t),\ t) \tag{11}$$

and extract the high-frequency part of Eqs. (6). With use of the inequalities (10), we easily obtain to the specified order of non-linearity, the coupled equations

$$\left(\frac{\partial}{\partial t} + \underset{\sim}{U}\cdot\nabla_s\right)\phi_s + g\zeta = 0\ ,$$

$$\left(\frac{\partial}{\partial t} + \underset{\sim}{U}\cdot\nabla_s\right)\zeta + \zeta\ \nabla_s\cdot\underset{\sim}{U} = \textcircled{\#}\phi_s \tag{12}$$

Here we have introduced the operator

$$\textcircled{\#} = \left(-\nabla_s^2\right)^{1/2} \tag{13}$$

and understand that it will always act on a Fourier series. Laplace's equation, $\nabla^2\hat{\phi}=0$, has been used to write

$$\left[\frac{\partial\phi}{\partial z} - (\nabla_s H)\cdot\nabla_s\phi\right]_{z=H} = \textcircled{\#}\,\phi_s + \mathcal{O}\left[\left(\nabla_s^2 H\right)\phi_s\right]$$

in the second of Eqs. (12).

We next extract the low frequency, long wavelength portion of Eq. (6). On following an argument of Phillips, [1966, Eq. (5.2.12)] we obtain with a little straightforward algebra the surface boundary condition

$$\left.\frac{\partial\Phi}{\partial z}\right|_{z=0} = \nabla_s\cdot\left\langle\zeta\nabla_s\ \phi_s\right\rangle_L\ . \tag{14}$$

Here we have written $\langle \Gamma \rangle_L$ as representing the "low frequency, long wavelength part" of the quantity Γ.

To continue, we suppose that in the absence of surface waves a complete set of eigenmodes for Eq. (7) are known to be of the form

$$w(\underset{\sim}{r},z,t) = W^o_{j,\underset{\sim}{L}}(z) \exp\left\{i\left[\underset{\sim}{L}\cdot\underset{\sim}{r} - \Omega(j,L)t\right]\right\} , \qquad (15)$$

where

$$W^o_{j,\underset{\sim}{L}}(0) = W^o_{j,\underset{\sim}{L}}(-H) = 0$$

Thus, $(j,\underset{\sim}{L})$ describes a free internal wave of mode number j [$j = 1,2,...$ in the notation of Garrett and Munk (1972a)] horizontal wave number $\underset{\sim}{L}$ and frequency $\Omega(j,L)$. The normalization of $W^o_{j,\underset{\sim}{L}}$ is so chosen that

$$\left[W^o_{j,\underset{\sim}{L}}(z)\right]' \Big|_{z=0} = L^2 . \qquad (16)$$

Here, and in the following, we write

$$F'(z) \equiv \frac{dF}{dz} ,$$

etc.

Equations (7) and (16) imply that in the mixed layer, where N=0, we can write

$$W^{o}_{j,\underset{\sim}{L}}(z) = - L \sinh (Lz) \quad , \quad -D < z < 0. \qquad (17)$$

At the thermocline $W^{o}_{j,\underset{\sim}{L}}$ is continuous, but

$$\left(W^{o}_{j,\underset{\sim}{L}}\right)' \Big|_{\text{above}} - \left(W^{o}_{j,\underset{\sim}{L}}\right)' \Big|_{\text{below}} = -g \frac{\delta\rho}{\rho_o} L^2 W^{o}_{j,\underset{\sim}{L}}(-D)/\Omega^2(j,L) .$$

Finally, in the range $-H < z < -D$, $W^{o}_{j,\underset{\sim}{L}}$ is found by integration of Eq. (7).

The above expression at the thermocline results in the dispersion relation

$$\Omega^2(j,L) = \left[(g\ \delta\rho/\rho_o) L\right] \Big/ \left[\mathcal{R}(j,L) + \coth(LD)\right] \quad , \qquad (18)$$

where

$$\mathcal{R}(j,L) = L^{-1}\left(\ell n\ W^{o}_{j,\underset{\sim}{L}}(z)\right)'$$

evaluated for z just below the thermocline.

To obtain the corresponding solutions to Eq. (7) with the surface boundary condition (14), we write (in the rectangular area A_o of ocean surface being considered)

$$\Phi(\underset{\sim}{r},z) = \sum_{j,\underset{\sim}{L}} \Phi_{j,\underset{\sim}{L}}(z)\ \exp(i\ \underset{\sim}{L}\cdot\underset{\sim}{r}),\ -D < z < 0 \ , \qquad (19)$$

and

$$w(\underset{\sim}{r},z) = \sum_{j,\underset{\sim}{L}} W_{j,\underset{\sim}{L}}(z)\ A_{j,\underset{\sim}{L}}(t)\ \exp(i\ \underset{\sim}{L}\cdot\underset{\sim}{r}) \quad . \qquad (20)$$

The form of Eq. (20) permits us to so normalize $W_{j,\underset{\sim}{L}}$ that

$$\Phi_{j,\underset{\sim}{L}}(0) = A_{j,\underset{\sim}{L}} \quad . \tag{21}$$

On writing, from Eq. (14),

$$\nabla_s \cdot \left\langle \zeta \nabla_s \phi_s \right\rangle_L \equiv \sum_{\underset{\sim}{L}} \Gamma_{\underset{\sim}{L}} \exp(i \underset{\sim}{L} \cdot \underset{\sim}{r}) \ ,$$

and on substituting this and the expansion (20) into Eq. (14), we obtain

$$W_{j,\underset{\sim}{L}}(0) \ A_{j,\underset{\sim}{L}} = \Gamma_{\underset{\sim}{L}} \quad . \tag{22}$$

Again, if we substitute the expansion (20) into Eq. (7), and (for the moment) drop the $(j,\underset{\sim}{L})$ labels, we obtain the equation

$$W'' + L^2 \left[N^2/\Lambda^2 - 1 \right] W = 0 \quad , \tag{23}$$

$$\Lambda^2 \equiv - \ddot{A}/A \quad ,$$

where $\dot{A} \equiv \frac{dA}{dt}$, etc.

We now consider $\Gamma_{\underset{\sim}{L}}$ to be small, ie., the vertical velocity of the internal wave is considered small with respect to the vertical variation of the free surface, and write,

(24)

$$W = W^{O} + \delta W \quad ,$$

$$\Lambda^2 = \Omega^2 + \delta\Lambda^2 \quad , \tag{24}$$

where W^{O} represents one of the eigenmodes (15) and Ω is one of the eigenfrequencies (18). Equation (22) can be re-expressed in the form

$$\delta WA = \Gamma \tag{25}$$

(ie., $W = 0$ at $z = 0$).

To obtain an equation for A(t), we consider the integral

$$J \equiv \int_{-H}^{O} W\left[W'' + L^2(N^2/\Lambda^2 - 1)W\right] dz = 0 \quad . \tag{26}$$

This integral is varied using Eq. (24) and can be written as $J = J^{O} + \delta J$, where J^{O} and δJ are, respectively, of order zero and one in the small quantity Γ. After some manipulation, the equation $\delta J = 0$ can be put into the form

$$\ddot{A} + \Omega^2 A = \left[\Omega^4 \Gamma \left(W^{O}(z)\right)'\Big|_{z=0}\right] \left[L^2 \int_{-H}^{0} N^2(z) \left(W^{O}(z)\right)^2 dz\right]^{-1} , \tag{27}$$

valid to first order in Γ.

To simplify the right-hand side of Eq. (27) [and putting back the (j,L) labels] it is convenient to define the quantity $g'(j,L)$ with the relation

$$\int_{-H}^{0} N^2(z)\left(W^{o}_{j,\underset{\sim}{L}}(z)\right)^2 dz \equiv g'(j,L)\left[W^{o}_{j,\underset{\sim}{L}}(-D)\right]^2$$

$$= L^2\, g'(j,L)\, \sinh^2(LD) \quad . \tag{28}$$

Equation (17) was used in the final step here. The expressions (16), (21) and (28) allow us to put Eq. (27) into the form

$$\ddot{\Phi}_{j,\underset{\sim}{L}}(0) + \Omega^2(j,L)\, \Phi_{j,\underset{\sim}{L}}(0)$$

$$= \Omega^4(j,L)\, \Gamma_{\underset{\sim}{L}} \Big/ \left[L^2 g'(j,L)\, \sinh^2(LD)\right]$$

$$\equiv C(j,L)\, \Gamma_{\underset{\sim}{L}} \quad . \tag{29}$$

We can formally return to the $\underset{\sim}{r}$ coordinate, defining [see Eq. (19)]

$$\Phi_j(\underset{\sim}{r}) \equiv \sum_{\underset{\sim}{L}} \Phi_{j,\underset{\sim}{L}}(o)\, \exp(i\underset{\sim}{L}\cdot\underset{\sim}{r}) \quad .$$

Then Eq. (29) can be re-written as

$$\ddot{\Phi}_j(\underset{\sim}{r}) + \Omega^2(j,\#)\, \Phi_j(\underset{\sim}{r}) = C(j,\#)\nabla_s \cdot \langle \zeta \nabla_s \phi_s \rangle_L \tag{30}$$

Here Ω and C are the appropriate operators to give Eq. (29) when the modal expansion is introduced.

The vertical displacement $\Xi(\underset{\sim}{r},t)$ at the thermocline is, in the linear approximation, obtained on integrating the equation

$$\Xi \equiv \sum_j \xi_j(\underset{\sim}{r},t)$$

$$\frac{\partial \xi_j}{\partial t} = \sum_{j,\underset{\sim}{L}} A_{j,\underset{\sim}{L}}\, W^{o}_{j,\underset{\sim}{L}}(-D)\, \exp(i\,\underset{\sim}{L}\cdot\underset{\sim}{r})$$

$$= - \sum_{j,\underset{\sim}{L}} L \sinh (LD)\ \Phi_{j,\underset{\sim}{L}}(0)\ \exp(i\ \underset{\sim}{L}.\underset{\sim}{r})$$

$$= \left[\frac{\sinh (D\textcircled{\#})}{D\textcircled{\#}}\right] D\ \nabla_s^2 \Phi_j(\underset{\sim}{r}) \quad . \tag{31}$$

Equations (12) and (30) represent coupled equations for interacting surface and internal waves. In the Appendix we show how to construct a system of Hamilton's equations equivalent to these. We shall just quote these equations here, using action-angle variables.

To do this, we write for the surface waves

$$\phi_s(\underset{\sim}{r},t) = \sum_{\underset{\sim}{k}} \left[\frac{2g\ J_{\underset{\sim}{k}}}{\rho_o\ \omega_k}\right]^{1/2} \cos(\underset{\sim}{k}\cdot\underset{\sim}{r} - \Theta_{\underset{\sim}{k}}) \quad ,$$

$$\zeta(\underset{\sim}{r},t) = -\sum_{\underset{\sim}{k}} \left[\frac{2\omega_k\ J_{\underset{\sim}{k}}}{\rho_o g}\right]^{1/2} \sin(\underset{\sim}{k}\cdot\underset{\sim}{r} - \Theta_{\underset{\sim}{k}}) \quad . \tag{32}$$

Here $\omega_k = (gk)^{1/2}$ is the angular frequency of a surface gravity wave of wavenumber $\underset{\sim}{k}$ in deep water. The quantity $J_{\underset{\sim}{k}}$ is the action per unit area of ocean surface for mode $\underset{\sim}{k}$ and $\Theta_{\underset{\sim}{k}}$ is the corresponding canonical angle variable.

The corresponding expansions for the internal waves are

$$\Phi_j(\underset{\sim}{r}) = \sum_{\underset{\sim}{L}} \left[\frac{2\Omega(j,L)\ J(j,\underset{\sim}{L})}{\rho_o\ T(j,L)}\right]^{1/2} \cos\left[\underset{\sim}{L}\cdot\underset{\sim}{r} - \Theta(j,\underset{\sim}{L})\right]$$

$$\Xi(\underset{\sim}{r},t) = \sum_{j,\underset{\sim}{L}} \left[\frac{2\Omega(j,L)\ J(j,\underset{\sim}{L})}{\rho_o g'(j,L)}\right]^{1/2} \sin\left[\underset{\sim}{L}\cdot\underset{\sim}{r} - \Theta(j,\underset{\sim}{L})\right] \quad . \quad (33)$$

Here,

$$T(j,L) \equiv \left[g'(j,L)L^2 \sinh^2(LD)/\Omega^2(j,L)\right]^{1/2} , \quad (34)$$

$J(j,\underset{\sim}{L})$ and $\Theta(j,\underset{\sim}{L})$ are the corresponding action-angle variables for internal waves and $g'(j,L)$ is given by the integral equation (28).

The Hamiltonian, referred to a unit area of ocean, is as obtained from Eq. (A.13) in the Appendix,

$$H = H_S + H_I + V \quad , \quad (35)$$

$$H_S = \sum_{\underset{\sim}{k}} J_{\underset{\sim}{k}}\ \omega_k \quad ,$$

$$H_I = \sum_{j,\underset{\sim}{L}} J(j,\underset{\sim}{L})\ \Omega(j,L)$$

$$V = -\sum_{\substack{\underset{\sim}{k},\underset{\sim}{n} \\ j,\underset{\sim}{L}}} \delta_{\underset{\sim}{k}-\underset{\sim}{n}-\underset{\sim}{L}}\ G(\underset{\sim}{k},\underset{\sim}{n};j,\underset{\sim}{L}) \left[J_{\underset{\sim}{k}}\ J_{\underset{\sim}{n}}\ J(j,\underset{\sim}{L})\right]^{1/2}$$

$$\times \sin\left[\Theta_{\underset{\sim}{k}} - \Theta_{\underset{\sim}{n}} - \Theta(j,\underset{\sim}{L})\right] \quad . \quad (36)$$

The quantity G here is

$$G(\underset{\sim}{k},\underset{\sim}{n};j,\underset{\sim}{L}) = \frac{1}{2\sqrt{2\rho_o}}\left[\frac{\Omega^{1/2}(j,L)}{T(j,L)}\right]\left[\left(\frac{\omega_n}{\omega_k}\right)^{1/2}\underset{\sim}{k}\cdot\underset{\sim}{L} + \left(\frac{\omega_k}{\omega_n}\right)^{1/2}\underset{\sim}{n}\cdot\underset{\sim}{L}\right] \quad (37)$$

Also, in writing Eq. (36) we have dropped as unimportant some rapidly oscillating terms involving $\sin\left[\theta_{\underset{\sim}{k}} + \theta_{\underset{\sim}{n}} + \theta(j,\underset{\sim}{L})\right]$.

Hamilton's equations are

$$\dot{J}_{\underset{\sim}{k}} = -\frac{\partial H}{\partial \theta_{\underset{\sim}{k}}} \quad , \quad \dot{\theta}_{\underset{\sim}{k}} = \frac{\partial H}{\partial J_{\underset{\sim}{k}}} \quad , \quad \text{etc.} \quad . \quad (38)$$

The angle variables in these equations occur in the combination

$$\phi(\underset{\sim}{k},j,\underset{\sim}{L}) \equiv \theta_{\underset{\sim}{k}} - \theta_{\underset{\sim}{k}-\underset{\sim}{L}} - \theta(j,\underset{\sim}{L}) \quad (39)$$

[note that the ϕ used here is not of Eq. (4)] and the resulting equations of motion are

$$\dot{J}_{\underset{\sim}{k}} = \sum_{j,\underset{\sim}{L}} 2\Big\{\hat{G}(\underset{\sim}{k},j,\underset{\sim}{L})\left[J_{\underset{\sim}{k}}\, J_{\underset{\sim}{k}-\underset{\sim}{L}}\, J(j,\underset{\sim}{L})\right]^{1/2}\cos\phi(\underset{\sim}{k},j,\underset{\sim}{L})$$

$$- \hat{G}(\underset{\sim}{k}+\underset{\sim}{L},j,\underset{\sim}{L})\left[J_{\underset{\sim}{k}+\underset{\sim}{L}}\, J_{\underset{\sim}{k}}\, J(j,\underset{\sim}{L})\right]^{1/2}\cos\phi(\underset{\sim}{k}+\underset{\sim}{L},j,\underset{\sim}{L})\Big\}$$

$$\dot{J}(j,\underset{\sim}{L}) = -\sum_{\underset{\sim}{k}} 2\,\hat{G}(\underset{\sim}{k},j,\underset{\sim}{L})\left[J_{\underset{\sim}{k}}\, J_{\underset{\sim}{k}-\underset{\sim}{L}}\, J(j,\underset{\sim}{L})\right]^{1/2}\cos\phi(\underset{\sim}{k},j,\underset{\sim}{L})$$

$$\dot{\phi}(\underset{\sim}{k},j,\underset{\sim}{L}) = \left[\omega_{\underset{\sim}{k}} - \omega_{|\underset{\sim}{k}-\underset{\sim}{L}|} - \Omega(j,\underset{\sim}{L})\right]$$

$$- \sum_{j',\underset{\sim}{M}} \left\{\hat{G}(\underset{\sim}{k},j;\underset{\sim}{M})\left[J_{\underset{\sim}{k}-\underset{\sim}{M}}\, J(j',\underset{\sim}{M})/J_{\underset{\sim}{k}}\right]^{1/2} \sin\phi(\underset{\sim}{k},j',\underset{\sim}{M})\right.$$

$$+\hat{G}(\underset{\sim}{k}+\underset{\sim}{M},j;\underset{\sim}{M})\left[J_{\underset{\sim}{k}+\underset{\sim}{M}}\, J(j',\underset{\sim}{M})/J_{\underset{\sim}{k}}\right]^{1/2} \sin\phi(\underset{\sim}{k}+\underset{\sim}{M},j',\underset{\sim}{M})$$

$$-\hat{G}(\underset{\sim}{k}-\underset{\sim}{L},j;\underset{\sim}{M})\left[J_{\underset{\sim}{k}-\underset{\sim}{L}-\underset{\sim}{M}} J(j',\underset{\sim}{M})/J_{\underset{\sim}{k}-\underset{\sim}{L}}\right]^{1/2} \sin\phi(\underset{\sim}{k}-\underset{\sim}{L},j',\underset{\sim}{M})$$

$$\left.-\hat{G}(\underset{\sim}{k}-\underset{\sim}{L}+\underset{\sim}{M},j;\underset{\sim}{M})\left[J_{\underset{\sim}{k}-\underset{\sim}{L}+\underset{\sim}{M}}\, J(j',\underset{\sim}{M})/J_{\underset{\sim}{k}-\underset{\sim}{L}}\right]^{1/2} \sin\phi(\underset{\sim}{k}-\underset{\sim}{L}+\underset{\sim}{M},j',\underset{\sim}{M})\right\}$$

$$+ \sum_{\underset{\sim}{p}} \hat{G}(\underset{\sim}{p},j,\underset{\sim}{L})\left[J_{\underset{\sim}{p}}\, J_{\underset{\sim}{p}-\underset{\sim}{L}}/J(j,\underset{\sim}{L})\right]^{1/2} \sin\phi(\underset{\sim}{p},j,\underset{\sim}{L}) \quad . \qquad (40)$$

In these equations we have written

$$\hat{G}(\underset{\sim}{k},j,\underset{\sim}{L}) \equiv G(\underset{\sim}{k},\underset{\sim}{k}-\underset{\sim}{L};j,\underset{\sim}{L}) \quad . \qquad (41)$$

The practicality of these equations of motion is demonstrable in that integration of the coupled, first order, ordinary differential equations has been achieved numerically to high accuracy with the simplest, first order Euler scheme.

In the absence of nonlinear coupling, the $J_{\underset{\sim}{k}}$ and $J(j,\underset{\sim}{L})$ are constant and $\Theta_{\underset{\sim}{k}} = \omega_{\underset{\sim}{k}} t$ + initial value, $\Theta(j,\underset{\sim}{L}) = \Omega(j,L)t$ + initial value, as is clear from Eq. (40). We see then from Eqs. (32) and (33) that our choice of variables is such that each linear mode corresponds to a progressive wave with

wavenumber vector $\underset{\sim}{k}, \underset{\sim}{L}$, etc. The expansions (32) and (33) may easily be modified to describe standing waves.

We conclude this section by noting that both H and the sum of the $J_{\underset{\sim}{k}}$'s are constants of the motion for our system. The total action being constant is a Manley-Rowe condition [see, for example, Sturrock (1960)]. The important implications of these two constants of the motion for energy exchange between two wave systems have been discussed, for example, by Cohen et al. (1972).

III. APPLICATIONS TO LABORATORY EXPERIMENTS

In the experiments of Lewis, Lake, and Ko (1974) an internal wave was mechanically driven at a fluid interface near the bottom of a wave tank. A small amplitude surface wave was also mechanically generated and the modulation by the internal wave of the surface wave height and slope recorded. The wavelengths of the surface waves were so selected that their group velocities were nearly equal to the phase velocity of the internal wave.

A theoretical calculation using perturbation theory was made by Lewis et al. (1974). This gave rather good agreement with their observations, but failed to show a saturation at the larger modulation amplitudes.

To apply our theory to this experiment we use the thin thermocline model [Eq. (3)] and adapt the choice of amplitude excitations [Eqs. (32) and (33)] to correspond to the standing waves generated in the tank. For the thin thermocline model only the lowest internal wave mode, corresponding to $j = 1$, occurs. Equations (40) were integrated with the initial condition that both internal and surface waves were simple standing waves at time $t = 0$. Surface wave sidebands developed as a result of the internal wave interaction and these caused an envelope modulation of the surface wave amplitude. The growth in time of this modulation was interpreted as a growth down the tank, assuming that the modulation was convected at the surface wave group velocity. The resulting modulation as

a function of distance down the tank is compared with the observations of Lewis et al. (1974) in Figure (1). The tendency of the modulation to saturate at about 22% should be noted.

In the above experiment of Lewis et al., the surface wave amplitudes were not large enough to significantly modify the internal wave. Another series of tank experiments to study explicitly the generation of internal waves by surface waves were performed by Joyce (1974).

For our present purposes, the experiment labeled E4 by Joyce is of primary interest. In this experiment Joyce created a fluid interface with a sharp density gradient approximately 30 cm below the surface of a 90 cm deep tank. Two standing waves were mechanically driven on the tank surface and allowed to interact. The experimental parameters were selected such that the interaction of the two standing surface waves would drive an internal wave as the third member of a resonant triad. The frequencies and amplitudes of the two standing waves were, respectively, 18.2003 and 17.7225 radians/sec and 0.377 cm and 0.268 cm. The growth of the resonant internal wave was observed.

A theoretical calculation of the resonant wave interaction using perturbation theory was performed by Joyce (1974). This agreed well with his observations at earlier times, but failed to show saturation at larger internal wave amplitudes.

To apply our theory to the Joyce experiment, we can again use the thin thermocline model of Eqs. (3). Viscous

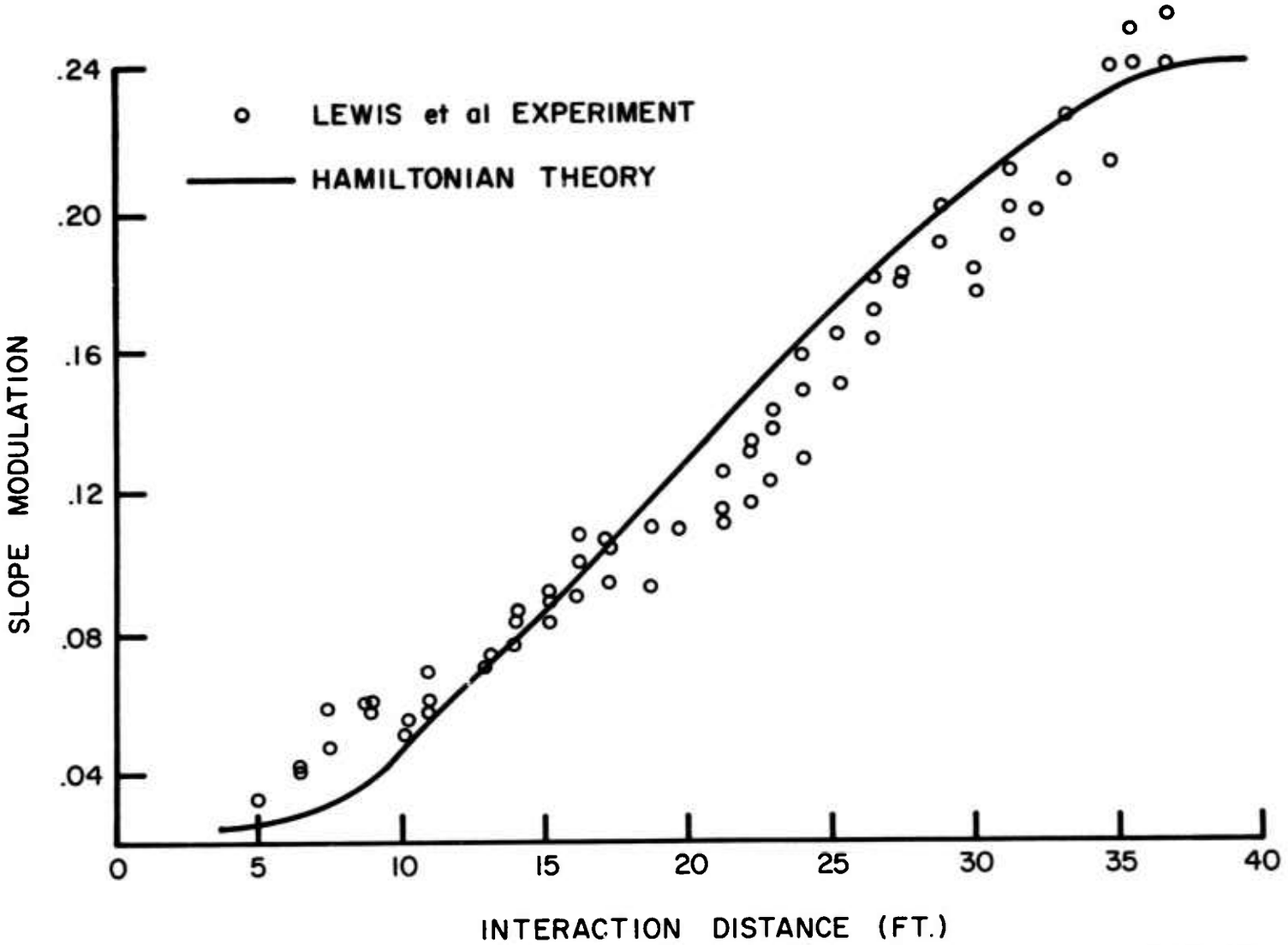
LEWIS et al EXPERIMENT
HAMILTONIAN THEORY
SLOPE MODULATION
.24
.20
.16
.12
.08
.04
0
5
10
15
20
25
30
35
40
INTERACTION DISTANCE (FT.)

XBL 752-189

damping terms must be added to the Eqs. (40) for $\dot{J}_{\underset{\sim}{k}}$ and $\dot{J}(1,\underset{\sim}{L})$, as described by Joyce (1974). The results of our calculation are shown in Figure 2, where they are compared with Joyce's measurements. The solid curve in Figure 2 was obtained assuming that the relative phase $\phi(\underset{\sim}{k},1,\underset{\sim}{L})$ was "locked," having the value π. The dashed curve results from integration of the complete set of Eqs. (40). The tendency for saturation to occur is seen to be more pronounced for the exact integration of Eqs. (40).

The "locked phase" approximation is often valid with fair accuracy in resonant triad interactions. Reference to the third of Eqs. (40) indicates that this approximation will fail catastrophically when the magnitude of the frequency mismatch becomes greater than the nonlinear coupling strength.

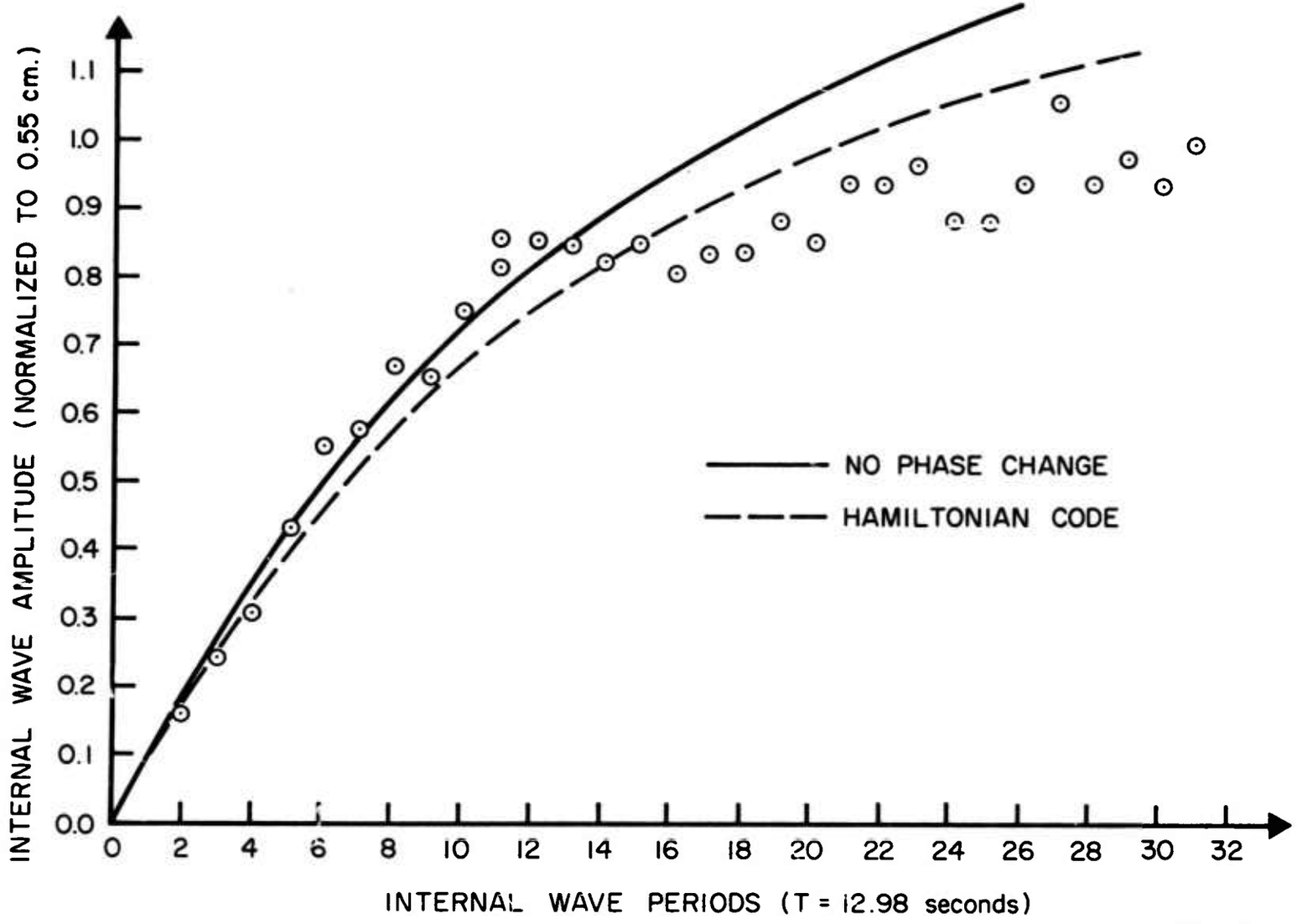
INTERNAL WAVE AMPLITUDE (NORMALIZED TO 0.55 cm.)
1.1
1.0
0.9
0.8
0.7
0.6
0.5
0.4
0.3
0.2
0.1
0.0
0
2
4
6
8
10
12
14
16
18
20
22
24
26
28
30
32
NO PHASE CHANGE
HAMILTONIAN CODE
INTERNAL WAVE PERIODS (T = 12.98 seconds)

XBL 752-190

IV. APPLICATIONS TO OCEAN WAVES

In this section we shall relate the formalism developed in Section II to ocean wave phenomena and discuss some consequences of Eq. (40).

The power spectrum $\Psi_s(\underset{\sim}{k})$ of ocean surface waves has been reviewed by Phillips (1966, pg 75). This spectrum is so normalized that

$$\sum_{\underset{\sim}{k}} \left(\frac{(2\pi)^2}{A_o} \right) \Psi_s(\underset{\sim}{k}) = \int d^2k \Psi_s(\underset{\sim}{k}) = \langle \zeta^2 \rangle \quad . \tag{42}$$

Here $\langle \ldots \rangle$ represents an ensemble average over many specific realizations of the ocean. For simplicity, we assume that $\langle \zeta^2 \rangle$ is independent of position on the ocean surface. In the writing of Eq. (42) we have replaced a sum over discrete modes in the surface region of area A_o by an integral over wavenumber.

The corresponding internal wave power spectrum $\Psi_I(j,\underset{\sim}{L})$ has been discussed by Garrett and Munk (1972a, 1975). The indicated arguments of Ψ_I are mode number j and wavenumber $\underset{\sim}{L}$. This spectrum is so normalized that

$$\sum_{j=1}^{\infty} \int d^2L \, \Psi_I(j,\underset{\sim}{L}) = \sum_{j=1}^{\infty} \langle \xi_j^2 \rangle = \langle \Xi^2 \rangle \tag{43}$$

which is here considered to be independent of $\underset{\sim}{r} = (x,y)$ and to be evaluated at $z = -D$, the thermocline depth.

These power spectra may be related to the action variables using Eqs (32) and (33). We first observe that

$$\langle \zeta^2 \rangle = \sum_{\underset{\sim}{k}} (g\rho_o)^{-1} J_{\underset{\sim}{k}} \omega_k$$

$$\langle \xi_j^2 \rangle = \sum_{\underset{\sim}{L}} \left[\rho_o g'(j,L)\right]^{-1} J(j,\underset{\sim}{L})\ \Omega(j,L)$$

Therefore,

$$J_{\underset{\sim}{k}} = (g\rho_o/\omega_k) \left[\frac{(2\pi)^2}{A_o}\right] \Psi_s(\underset{\sim}{k})$$

$$J(j,\underset{\sim}{L}) = \left[g'(j,L)\rho_o/\Omega(j,L)\right] \left[\frac{(2\pi)^2}{A_o}\right] \Psi_I(j,\underset{\sim}{L}) \quad . \quad (44)$$

The equilibrium spectrum suggested by Phillip's (1966) is of the form,

$$\Psi_s(\underset{\sim}{k}) = 4x10^{-3}\ k^{-4}\ G_s(k,\beta)h(k) \quad , \quad k_s > k > k_o$$

$$h(k) = 1 \quad \text{for } k_s > k > k_o$$

$$= 0 \quad \text{for } k < k_o \quad \text{or} \quad k > k_s \quad . \quad (45)$$

Phillips (1966) chose

$$G_s(k,\beta) = \frac{1}{\pi} \quad \text{for} \quad \hat{\underset{\sim}{k}}\cdot\hat{\underset{\sim}{w}} \equiv \cos\beta > 0$$

$$=0 \quad \text{for} \quad \hat{\underset{\sim}{k}}\cdot\hat{\underset{\sim}{w}} < 0 \quad (46)$$

where $\hat{\underset{\sim}{w}}$ is a unit vector in the direction the wind is blowing. The spectrum suggested by Garrett and Munk (1975) is for internal waves with mode corresponding to j=1:

$$\Psi_I(j,\underset{\sim}{L}) = 8.0\times10^{-3}\ L \Big/ \left[\left(L^2 + 1.14\times10^{-9} j^2\right)^2 (j+6)^{2.5}\right]. \quad (47)$$

Were the nonlinear interactions responsible for energy exchange among the linear modes sufficiently strong, we might expect on statistical grounds <u>equipartion</u> of energy with

$$\omega_k J_{\underset{\sim}{k}} = \Omega(j,L)J(j,\underset{\sim}{L}) = \text{const. all } \underset{\sim}{k} \text{ and } \underset{\sim}{L} \quad .$$

This condition is, of course, grossly violated because dissipation and generation mechanisms overwhelm the tendency to equipartition the energy. The energy per mode per unit area, $\omega_k J_{\underset{\sim}{k}}$ and $\Omega(1,L)J(1,\underset{\sim}{L})$, is shown in Fig. (3) as a function of wavenumber, using Eqs. (44), (45) and (47), and assuming a "rectangular ocean" of dimensions 100 km × 100 km and the Garrett-Munk ocean model (2) with D = 100 m and $\delta\rho/\rho_o = 10^{-3}$.

In the remainder of this paper we shall study the implications of Eqs. (44) for the generation of internal waves by surface waves. We can assume that appreciable exchange of energy will occur only among "resonant triads" satisfying the condition that [See the third of Eqs. (40).]

$$\Delta\omega \equiv \left[\omega_k - \omega_{|\underset{\sim}{k}-\underset{\sim}{L}|} - \Omega(j,L)\right] \quad \text{is small.} \quad (48)$$

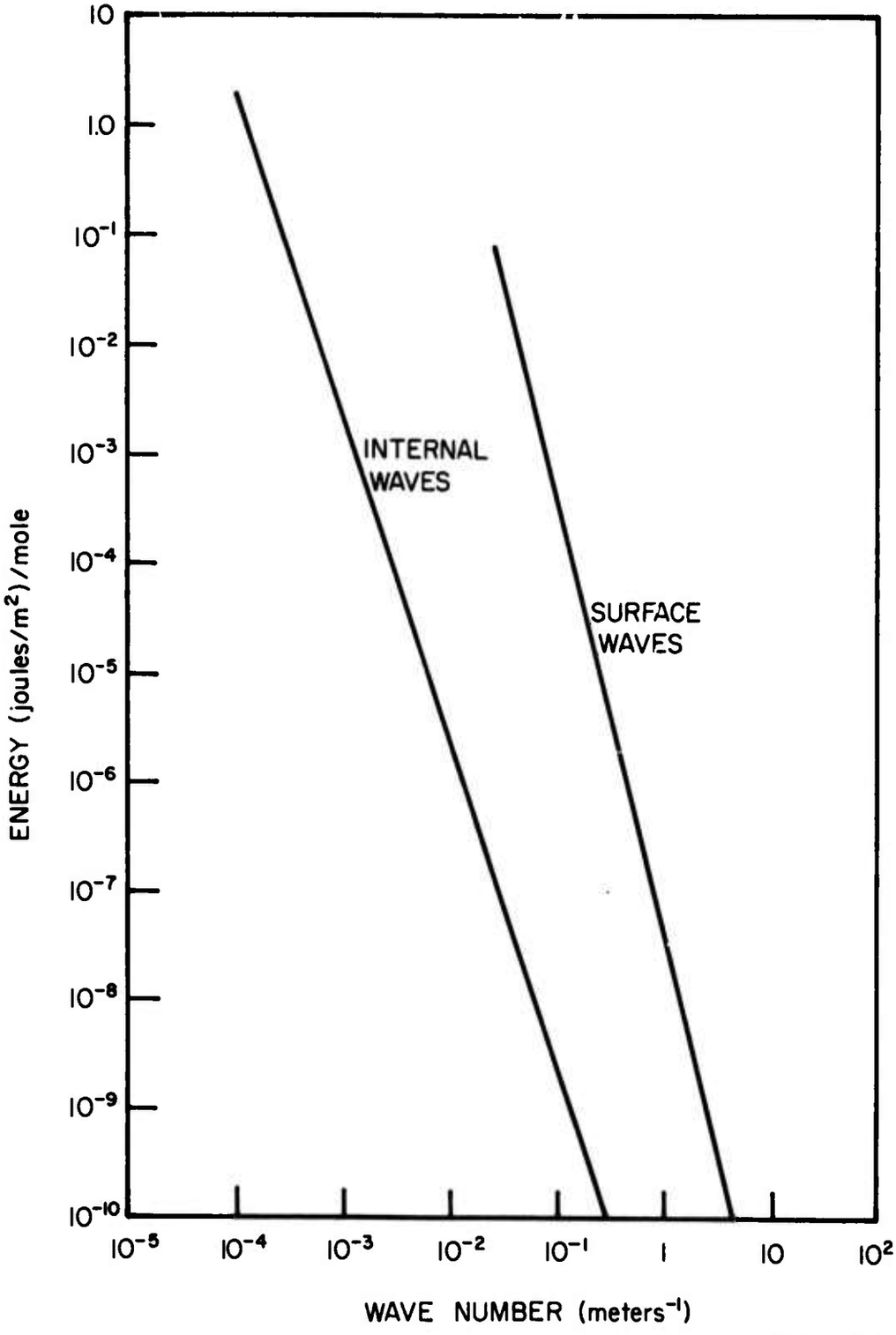
10
1.0
10^{-1}
10^{-2}
10^{-3}
10^{-4}
10^{-5}
10^{-6}
10^{-7}
10^{-8}
10^{-9}
10^{-10}
ENERGY (joules/m^2)/mole
INTERNAL WAVES
SURFACE WAVES
10^{-5}
10^{-4}
10^{-3}
10^{-2}
10^{-1}
1
10
10^2
WAVE NUMBER (meters^{-1})

XBL 752-271

In practice this condition is that $\Delta\omega$ be not significantly larger than the other term on the right in the third equation of Eq. (40).

We first describe numerical integration of Eqs. (40) for three simple examples. For each of these we have taken D = 100 m and $\delta\rho/\rho_o = 10^{-3}$ and use the thin thermocline model of Eq. (3). A single internal wave mode of wavenumber $\underset{\sim}{L}$ interacts with three surface wave modes, 1, 2, 3, of respective wavenumbers

$$\underset{\sim}{k}_1 \ , \quad \underset{\sim}{k}_2 = \underset{\sim}{k}_1 - \underset{\sim}{L} \quad , \quad \underset{\sim}{k}_3 = \underset{\sim}{k}_2 - 2\underset{\sim}{L} \quad . \tag{49}$$

The initial phases ϕ , at t = 0, were all set equal to zero in Eqs. (40).

For the first example we have suppressed mode 3 in Eq. (49) and have taken (in polar coordinates) the values listed under I in Table I corresponding to exact resonance. The rms amplitudes of the three modes (i.e., $\sqrt{\langle\zeta^2\rangle}$ or $\sqrt{\langle\Xi^2\rangle}$) are shown in Fig. (4) as a function of time. The initial decrease in amplitude of the internal wave mode is a consequence of our choice of initial condition that the phases ϕ vanish at t = 0. As $J(1,\underset{\sim}{L})$ reaches its minimum value, the phase $\phi(\underset{\sim}{k},1,\underset{\sim}{L})$ switches to the value π, and $J(1,\underset{\sim}{L})$ begins to increase. Although not shown in the figure, the internal wave amplitude reaches a maximum of 10.9 m at 1.7×10^4 sec and then begins to decrease.

TABLE I

WAVE VECTOR	I	II	III
$\underset{\sim}{k}_1$	(.03 m^{-1},0°)	(.03 m^{-1}0°)	(.03 m^{-1},0°)
$\underset{\sim}{k}_2$	(.0298 m^{-1},-3.8°)	(.02964 m^{-1},-7.7°)	(.029896 m^{-1},1.9°)
$\underset{\sim}{k}_3$	-------	(.029812 m^{-1},-15.4°)	(.029824 m^{-1},-3.8°)
$\underset{\sim}{L}$	(.002m^{-1}, 82.3°)	(.004 m^{-1},81°)	(.001 m^{-1},83°)
$\lvert\Delta\omega_{12}\rvert$	1.81×10^{-3} sec^{-1}	3.29×10^{-3} sec^{-1}	9.44×10^{-4} sec^{-1}
$\lvert\Delta\omega_{13}\rvert$	-------	1.58×10^{-3} sec^{-1}	1.59×10^{-3} sec^{-1}
$\lvert\Delta\omega_{23}\rvert$	-------	1.58×10^{-3} sec^{-1}	6.48×10^{-4} sec^{-1}

The wavevectors for three surface modes $\underset{\sim}{k}_1$, $\underset{\sim}{k}_2$ and $\underset{\sim}{k}_3$ and a single internal wave ($\underset{\sim}{L}$) for three example calculations are listed. Also the absolute frequency difference between the surface modes taken two at a time are listed.

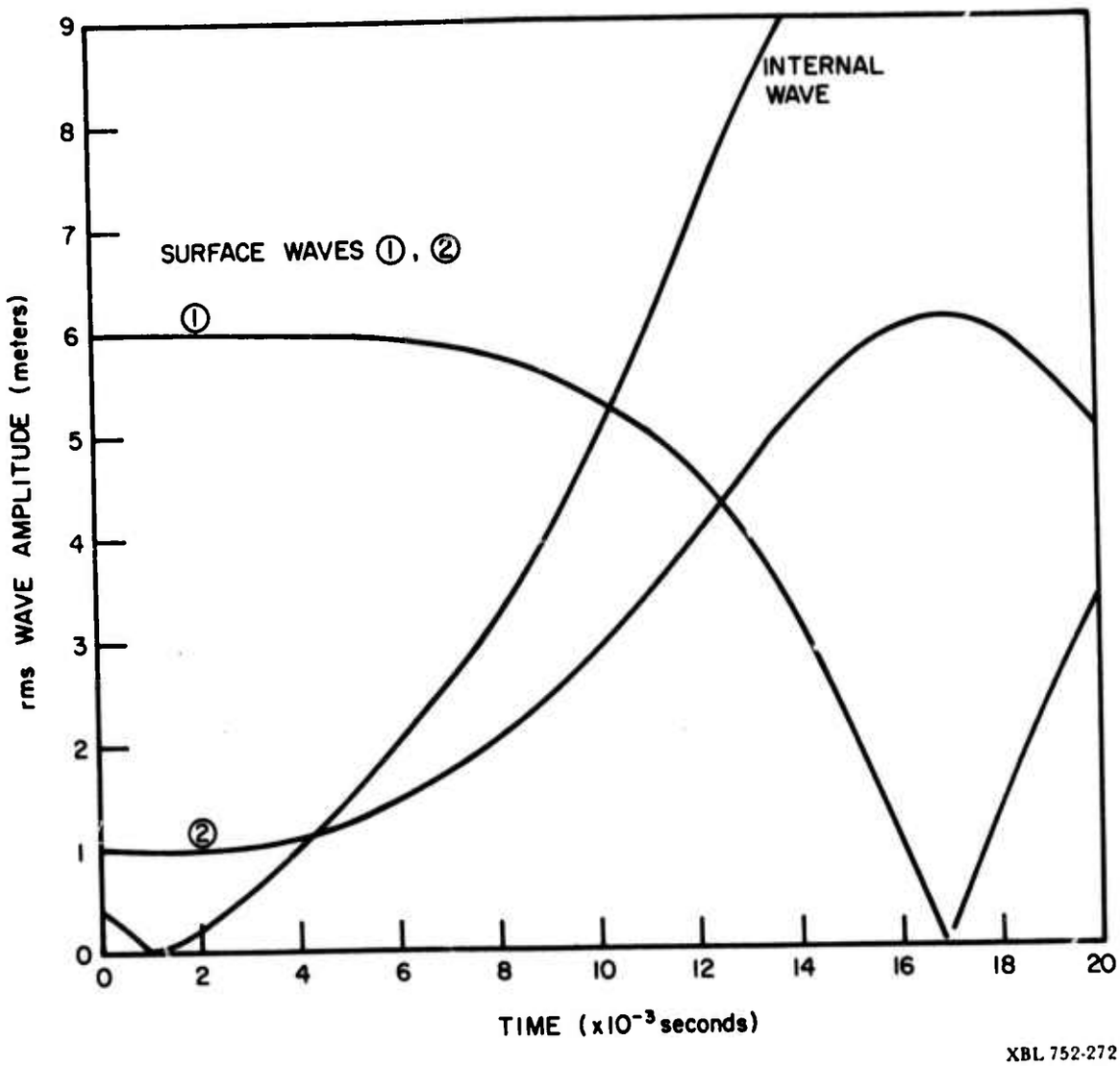
INTERNAL
WAVE
SURFACE WAVES ①, ②
①
②
rms WAVE AMPLITUDE (meters)
TIME (x10⁻³ seconds)
0
1
2
3
4
5
6
7
8
9
0
2
4
6
8
10
12
14
16
18
20

XBL 752-272

For the next example, we have chosen the modes corresponding to column II in Table I. The frequency differences are also listed and we observe that $\Delta\omega_{12}(\equiv \omega_{k_1} - \omega_{k_2}) = \Omega(1,L)$. The resulting rms wave amplitudes are shown as a function of time in Fig. (5). The amplitude of mode 3 is seen to be nearly constant (to within less than one percent). The reason for this is that it is too far from resonance (but not far enough to completely lose resonant effects).

For our third example we have chosen the modes with wavenumbers listed in column III of Table I with the frequency differences as shown. Note that again, $\Delta\omega_{12} = \Omega(1,L)$. The resulting rms wave amplitudes are shown as functions of time in Fig. (6). The frequency difference $\Delta\omega_{23}(\equiv \omega_{k_2} - \omega_{k_3})$ is now close enough to resonance that significant coupling to mode 3 occurs after the mode 2 amplitude has reached about 4 m.

Our third example suggests the following generalization. If we write

$$\underset{\sim}{k}_n = \underset{\sim}{k}_1 - (n-1)\underset{\sim}{L},\ n = 2,\ 3,\ \ldots\ , \tag{50}$$

and assume

$$nL << k_1, \text{ all n's considered,}$$

then

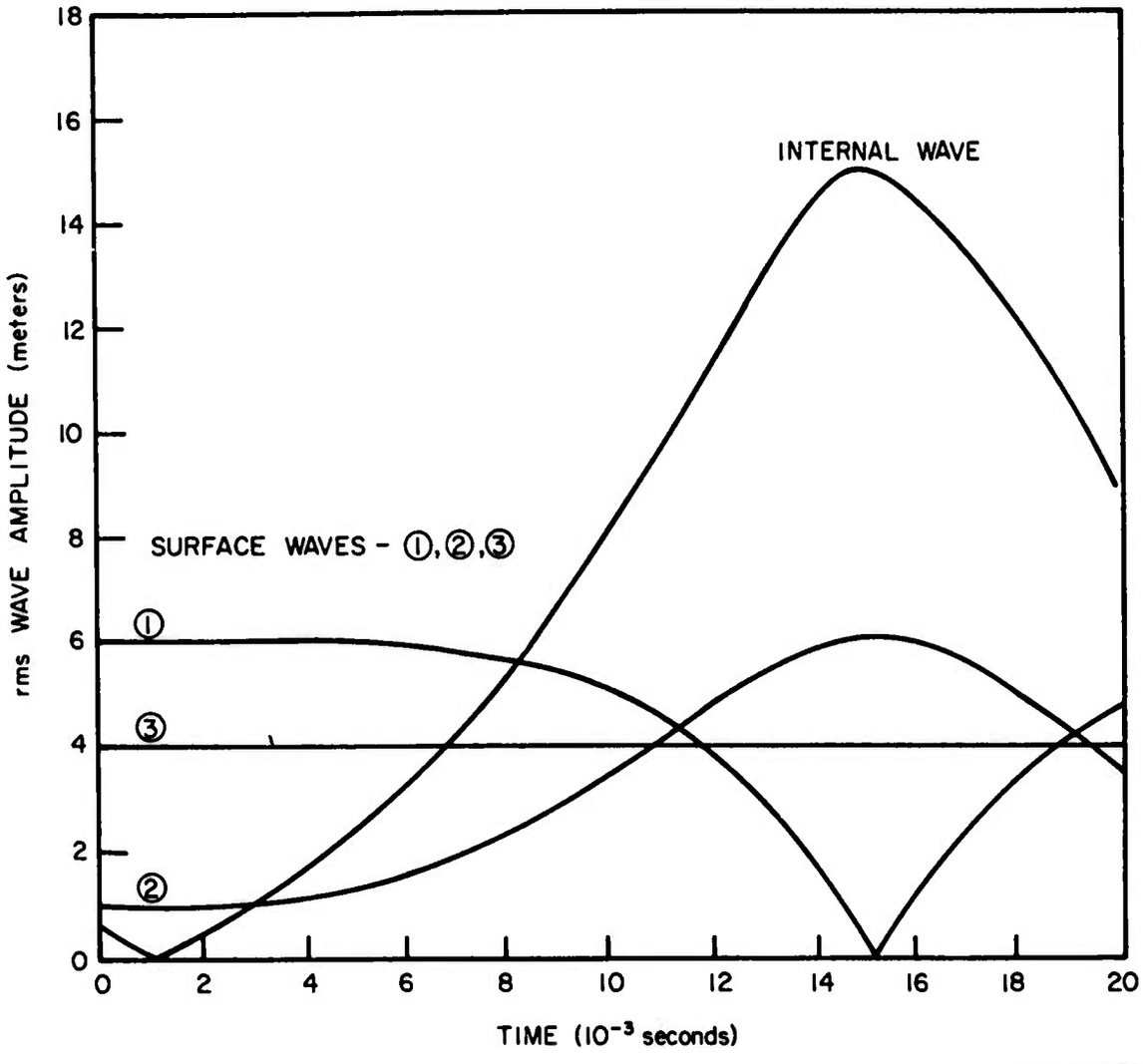
INTERNAL WAVE
SURFACE WAVES - ①,②,③
①
③
②
rms WAVE AMPLITUDE (meters)
TIME (10^{-3} seconds)
0
2
4
6
8
10
12
14
16
18
20

XBL 752-273

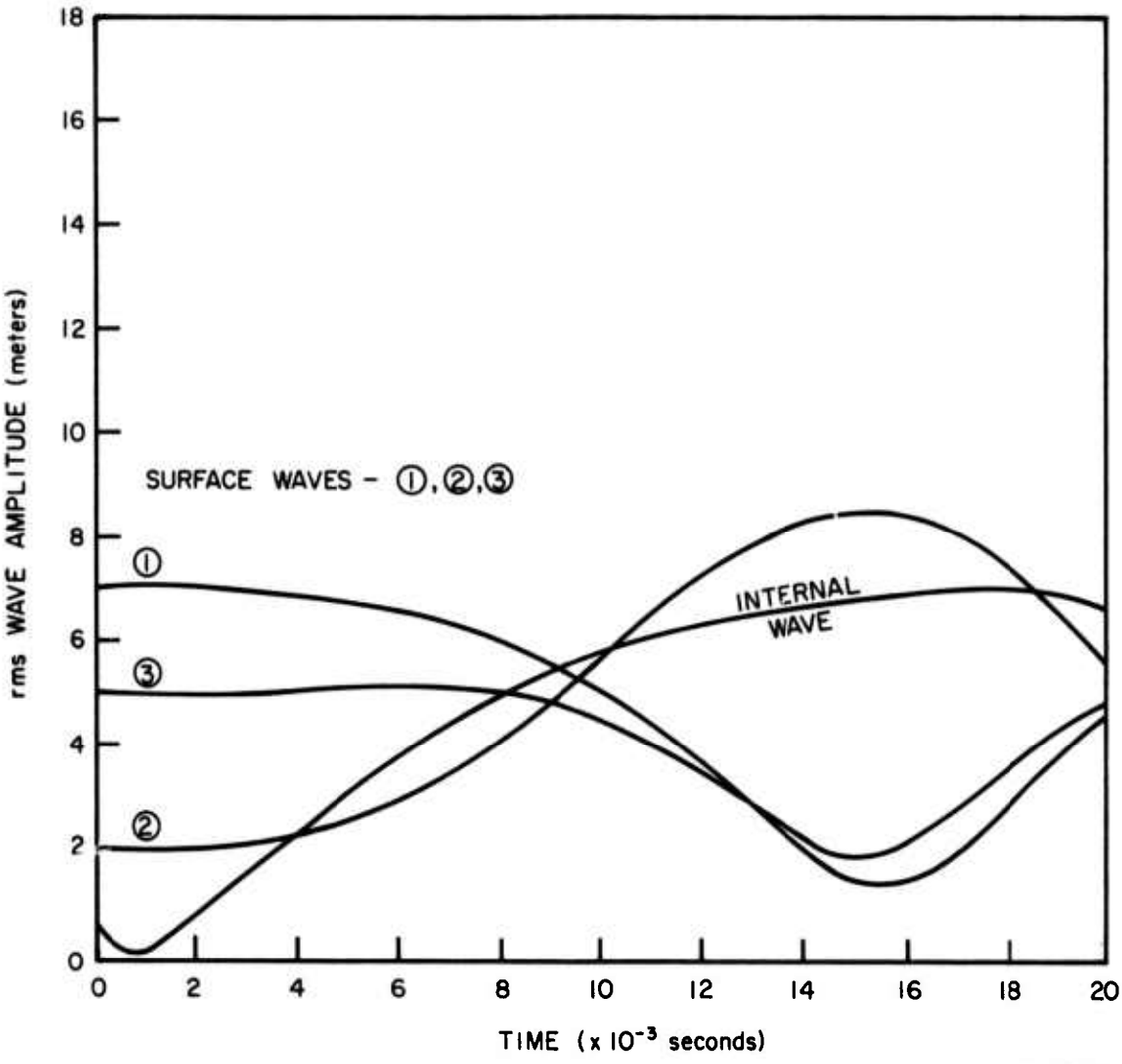
rms WAVE AMPLITUDE (meters)
18
16
14
12
10
8
6
4
2
0
SURFACE WAVES - ①,②,③
①
③
②
INTERNAL WAVE
0
2
4
6
8
10
12
14
16
18
20
TIME (x 10⁻³ seconds)

XBL 752-274

$$\omega_{k_{n-1}} - \omega_{k_n} \cong \underset{\sim}{C}_{\underset{\sim}{k}_1} \cdot \underset{\sim}{L} \quad ,$$

where $\underset{\sim}{C}_{\underset{\sim}{k}_1}$ is the group velocity of mode 1. Now if

$$\Omega(1,L) \cong \underset{\sim}{C}_{\underset{\sim}{k}_1} \cdot \underset{\sim}{L} \tag{51}$$

we satisfy the resonance condition between the internal wave and adjacent pairs of surface waves. In this case, a "cascade" process of energy exchange can result, just as has been noted for laser-plasma wave couplings [See Cohen, Kaufman, and Watson (1972)].

We next study the transfer of excitation from a sharply collimated spectrum of surface waves to internal waves. By "sharply collimated," we mean that the function $G_s(k,\beta)$ in Eq. (45) vanishes unless $\beta \cong \beta_o$, a constant. The excitation of a single internal wave mode $(j,\underset{\sim}{L})$, having a very small action variable $J(j,\underset{\sim}{L})$ will be considered. The energy source for driving this internal wave mode will be a set of large amplitude surface waves having wavenumbers $\underset{\sim}{p}_1$, $\underset{\sim}{p}_2$, ... and corresponding action variables $J^o_{\underset{\sim}{p}_1}$, $J^o_{\underset{\sim}{p}_2}$, ... The set of waves consisting of the third members of resonant triads are surface waves of small amplitude having wavenumbers $\underset{\sim}{k}_i = \underset{\sim}{p}_i - \underset{\sim}{L}$ and respective action variables $J_{\underset{\sim}{k}_i}$ (i=1,2,...). We shall assume that the large amplitude quantities $J^o_{\underset{\sim}{p}_i}$ are constant

during the time of interaction [The approximation of parameteric amplification, see for example, Nishikawa (1968)]. The "locked phase" approximation will also be used, so Eqs. (40) now read

$$\dot{J}_{\underset{\sim}{k}_i} = 2\,\hat{G}(\underset{\sim}{p}_i, j, \underset{\sim}{L})\left[J^o_{\underset{\sim}{p}_i}\, J_{\underset{\sim}{k}_i}\, J(j,\underset{\sim}{L})\right]^{1/2},$$

$$\dot{J}(j,\underset{\sim}{L}) = \sum_i 2\,\hat{G}(\underset{\sim}{p}_i, j, \underset{\sim}{L})\left[J^o_{\underset{\sim}{p}_i}\, J_{\underset{\sim}{k}_i}\, J(j,\underset{\sim}{L})\right]^{1/2},$$

$$\cos\phi(\underset{\sim}{p}_i, j, \underset{\sim}{L}) = -1, \text{ all modes.} \qquad (52)$$

We look for a solution to these equations of the form

$$J_{k_i} = C_i \exp(\alpha t)$$

$$J(j,\underset{\sim}{L}) = D \exp(\alpha t) \qquad (53)$$

and find that

$$\alpha^2 = \sum_i \left[2\,\hat{G}(\underset{\sim}{p}_i, j, \underset{\sim}{L})\right]^2 J^o_{\underset{\sim}{p}_i} .$$

Using the first of Eqs. (44) and transforming from the discrete to the continuous system we can re-express α^2 as an integral over the surface wave spectrum:

$$\alpha^2 = \int d^2k \left[(4\, g\rho_o)/\omega_k\right]\left[\hat{G}(\underset{\sim}{k}, j, \underset{\sim}{L})\right]^2 \Psi_s(\underset{\sim}{k}) . \qquad (54)$$

To simplify Eq. (54) we use the assumed condition that $L << k$ and Eqs. (37) and (41) to write

$$\hat{G}^2(\underset{\sim}{k},j,\underset{\sim}{L}) \cong \frac{2\Omega(j,L)}{\rho_o T^2(j,L)} \left[\underset{\sim}{k}\cdot\underset{\sim}{L} - \frac{1}{2}L^2\right]^2 .$$

Now the resonance condition

$$f = \omega_{|\underset{\sim}{k}-\underset{\sim}{L}|} \quad , \quad f \equiv \omega_k - \Omega(j,L) \quad , \tag{55}$$

lets us write

$$\underset{\sim}{k}\cdot\underset{\sim}{L} = \frac{1}{2}\left[k^2 + L^2 - f^4/g^2\right], \tag{56}$$

or

$$\left[\underset{\sim}{k}\cdot\underset{\sim}{L} - \frac{1}{2}L^2\right]^2 \cong 4k^3\,\Omega^2(j,L)/g \quad .$$

Collecting these results, and using the spectral representation (45), we can write Eq. (54) in the form

$$\alpha^2 = \left[\frac{\varrho\Omega^5(j,L)\,(4\times10^{-3})}{g'(j,L)\;L^2\;\sinh(LD)}\right]\int\frac{dk}{\omega_k}\,h(k)\int d\beta\;G_s(k,\beta) \tag{57}$$

The observations of Tyler, et al. (1974), suggest that the spectral angular distribution $G_s(k,\beta)$ [Eq. (45)] is strongly peaked near the long wavelength cut-off and in the direction the wind is blowing. If a modification of the Phillips spectrum (45) is desired, (for example, to describe a swell) an appropriate function $h(k)$ may be used in Eq. (57).

Now, Eq. (55) implies that for $k \simeq k_o$; $\underset{\sim}{k}$ and $\underset{\sim}{L}$ are nearly perpendicular, so we might anticipate that a well collimated beam of surface waves would generate internal waves propagating at nearly right angles to the direction of the surface waves. Apel et al. (1975a) have, indeed, reported what seems to be internal waves generated by a large swell and propagation at nearly right angles to the swell.

To model this, we take $G_s(k,\beta) = \delta(\beta)$ and evaluate the integral in Eq. (57) as

$$\int \frac{dk}{\omega_k} h(k) \int d\beta \; G_s(k,\beta) \equiv \frac{1}{V_c} \quad , \tag{58}$$

where V_c is a "characteristic velocity."

We have taken $V_c = 20$ m/sec† and evaluated α for the first four modes ($j = 1,\ldots 4$) using the Garrett-Munk ocean model Eq. (2).* The results for $1/\alpha$ in seconds are shown in Fig. (7) as a function of internal wavenumber L for a mixed layer depth of 100 m. The solid curves correspond to $\delta\rho/\rho_o = 0$, the dashed curves to $\delta\rho/\rho_o = 10^{-3}$ at the thermocline.

The lowest order internal wavemodes are excited much more strongly than are the higher modes. Since the lower modes are concentrated nearer the ocean surface this is not unexpected.

---

†Since α varies as $1/\sqrt{V_c}$ the curves in Fig. (7) are easily re-scaled for other values of V_c.

*The WKB approximation was used to find the eigenmodes (15).

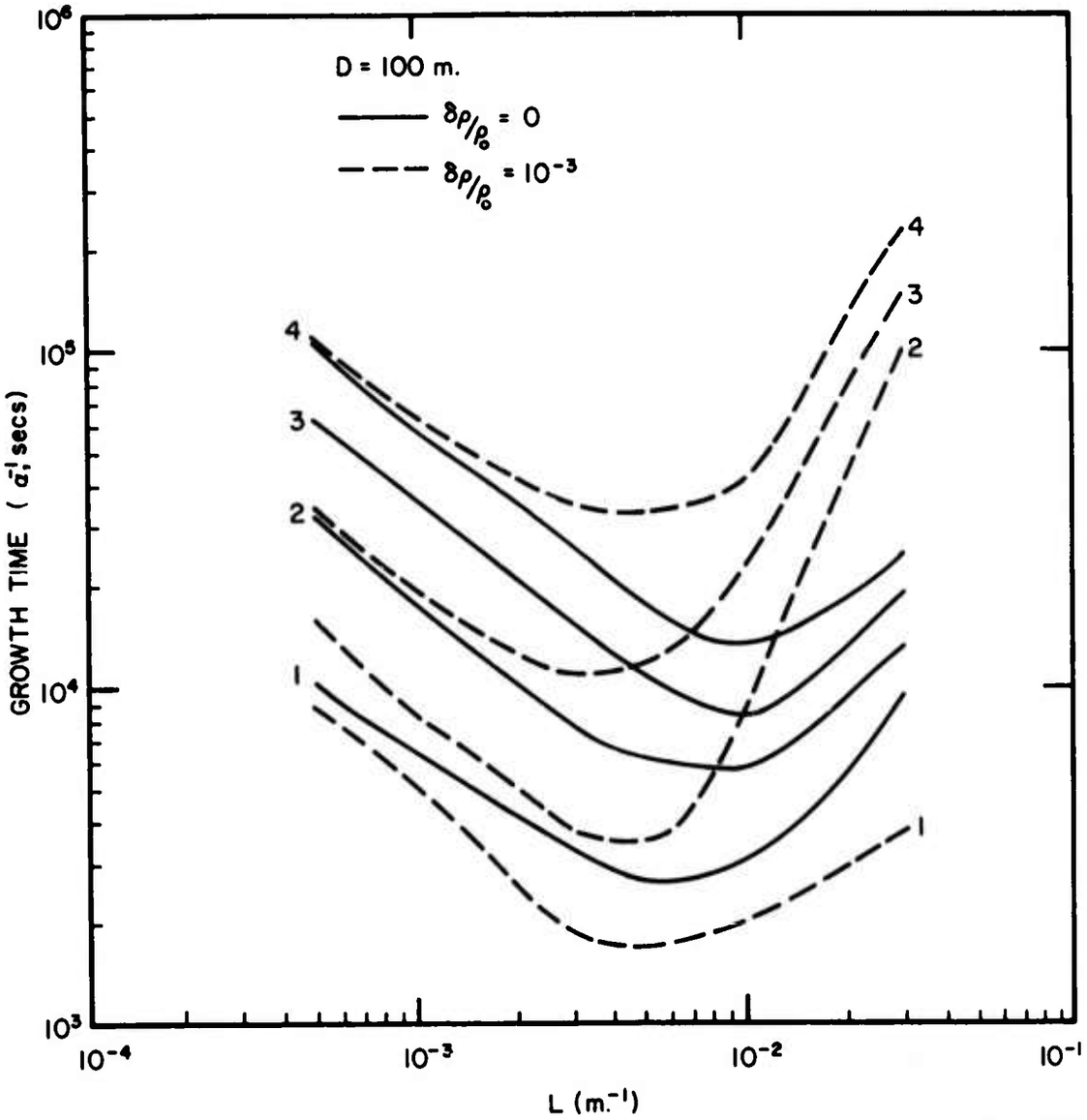
D = 100 m.
$\delta\rho/\rho_o = 0$
$\delta\rho/\rho_o = 10^{-3}$
GROWTH TIME (α^{-1}; secs)
L ($m.^{-1}$)
10^6
10^5
10^4
10^3
10^{-4}
10^{-3}
10^{-2}
10^{-1}
1
2
3
4

XBL 752-277

Some insight into the validity of the "locked phase" and "parametric amplification" approximation will be found in the next section, where numerical integration of Eqs. (40) is studied.

V. GENERATION OF INTERNAL WAVES FROM A SATURATED SURFACE SPECTRUM

In this section we shall study the generation of a specific internal wave mode $(j,\underset{\sim}{L})$ by a saturated surface wave spectrum. For this we use the expression (45) with $G_s(k,\beta)$ given by Eq. (46). Since the spectrum (45) is isotropic over a hemisphere, the generated internal wave spectrum will be approximately isotropic. A set of interacting triads will have surface wavenumbers $\underset{\sim}{p}_i$ and $\underset{\sim}{k}_i = \underset{\sim}{p}_i - \underset{\sim}{L}$, $i = 1, 2, \ldots$.

To simplify notation, we write

$$\Omega \equiv \Omega(j,L) \quad , \quad G_i \equiv \hat{G}(\underset{\sim}{p}_i, j, \underset{\sim}{L}) \quad ,$$

$$\phi_i \equiv \phi(\underset{\sim}{p}_i, j, \underset{\sim}{L}) \, , \quad J \equiv J(j, \underset{\sim}{L}) \quad .$$

Then, for the set of interacting triads Eqs. (40) can be written in the form

$$\dot{J}_{\underset{\sim}{k}_i} = -2\, G_i \left[J_{\underset{\sim}{p}_i}\, J_{\underset{\sim}{k}_i}\, J \right]^{\frac{1}{2}} \cos\phi_i = -\dot{J}_{\underset{\sim}{p}_i} \quad ,$$

$$\dot{J} = \sum_i \dot{J}_{\underset{\sim}{k}_i}$$

$$\dot{\phi}_i = \omega_{p_i} - \omega_{k_i} - \Omega$$

$$- G_i \sin\phi_i \left[\left(\frac{J_{\underset{\sim}{k}_i}}{J_{\underset{\sim}{p}_i}} \right)^{\frac{1}{2}} - \left(\frac{J_{\underset{\sim}{p}_i}}{J_{\underset{\sim}{k}_i}} \right)^{\frac{1}{2}} \right] \sqrt{J}$$

$$+ \sum_n G_n \left[\frac{J_{\underset{\sim}{p}_n} J_{\underset{\sim}{k}_n}}{J} \right]^{\frac{1}{2}} \sin\phi_n \quad . \tag{59}$$

The resonance condition (55) can be satisfied for $p_i < p_c$, the wavenumber at which the surface wave group velocity is equal to the internal wave phase velocity:

$$p_c = (gL^2)/(4\Omega^2) \quad . \tag{60}$$

Thus, we include only those modes in Eqs. (59) for which $p_c > p_i > k_o$ [Eq. (45)].*

Exact resonance is not required in Eqs. (59) for significant transfer of excitation. To take account of this, we set

$$\omega_{p_i} - \omega_{k_i} - \Omega = - \delta f \quad ,$$

where δf represents the frequency mismatch. Now, Eq. (56) becomes, for a given wavenumber $\underset{\sim}{p}$,

$$\underset{\sim}{p} \cdot \underset{\sim}{L} \equiv pL \cos\beta = \frac{1}{2} \left[k^2 + L^2 - (f + \delta f)^4/g^2 \right] \quad .$$

At exact resonance, corresponding to $\delta f = 0$, the angle β is

---

*For our numerical examples presented later it can be verified that p_c lies below the range of capillary wavenumbers.

β_r, where

$$\sin\beta_r \cong \left[1 - p/p_c\right]^{\frac{1}{2}} \quad . \tag{61}$$

For $\delta f \neq 0$, we have $\beta = \beta_r + \delta\beta$, where

$$\delta\beta \cong (2\,\omega_p\,\delta f)/(gL\,\sin\beta_r) \quad . \tag{62}$$

The mode index "i" in Eqs. (59) thus labels a magnitude and a direction for each $\underset{\sim}{p}_i$.

Integration of Eqs. (59) is simplified by introducing dimensionless variables, as follows:

$$J_{\underset{\sim}{p}_i} = J^o_{\underset{\sim}{p}_i}\; Z_i$$

$$J_{\underset{\sim}{k}_i} = J^o_{\underset{\sim}{k}_i}\; X_i \quad ,$$

$$J = J_o\; Y \quad ,$$

where [see Eqs. (44)]

$$J^o_{\underset{\sim}{p}_i} = (g\rho_o/\omega_{p_i})\left[\frac{(2\pi)^2}{A_o}\right]\Psi_s(\underset{\sim}{p}_i) \cong J^o_{\underset{\sim}{k}_i}$$

$$\therefore J_o = \left[\frac{\rho_o\, g'(j,L)}{\Omega}\right]\Xi_o^{\,2} \quad . \tag{63}$$

Here Ξ_o has the dimensions of length and is to be determined by the condition (65) below. A dimensionless time τ is introduced by the relation

$$t = \alpha^{-1}\tau \ ,$$

where α is defined, as in Section IV, by the equation

$$\alpha^2 = \sum_i \left[2\ G_i\right]^2 J^o_{\underset{\sim}{p}_i} \ . \tag{64}$$

The constant Ξ_o is then defined by the relation

$$2\ G_i\ J_o^{\frac{1}{2}} = \alpha(p_i/p_c)^{\frac{3}{2}} \ . \tag{65}$$

This takes proper account of the dependence of G_i on p_i.

The scaling (63) for the action variables implies that for the assumed saturated surface wave spectrum the initial values of the X_i and Z_i should be near unity.

To evaluate α^2, we can start with the expression (57). If we make the arbitrary, but reasonable, assumption that

$$|\delta f| \leq \alpha \ ,$$

then Eq. (62) can be used to give

$$\int d\beta\, G_s(p,\beta) = (4\omega_p\alpha)/(\pi g L \sin\beta_r) .$$

Integration over wavenumber, with the upper limit p_c, (the lower limit k_o can be taken to be zero for the present integration) gives

$$\alpha = \frac{8\left[4\times10^{-3}\right]\Omega^3}{\pi g'(j,L)\, L \sinh(LD)} \qquad (66)$$

The adopted scaling of variables in Eqs. (59) leads to coefficients of order unity, removing the coupling strengths G_i and the dimensional quantities $J^o_{p_i}$ and J_o. Writing

$$\frac{(2\pi)^2}{A_o} = \delta p_x\, \delta p_y = p\delta p \cdot \delta\beta \quad ,$$

lets us carry out the mode number sums as a numerical integration.

Equation (59) was numerically integrated with the Z_i and X_i initially equal to unity (changing initial conditions showed this to be uncritical). Nine values for β and eight for p_i were used making a total of seventy-two modes in Eq. (59). [Integration with fewer modes seemed to indicate little sensitivity to the number of modes used.]

A characteristic growth time τ_g for the internal wave mode was defined as

$$\tau_g = Y \Big/ \left[\frac{dY}{dt}\right] \quad ,$$

evaluated at that time τ that maximum power was being delivered

to the internal wave [i.e., $\dot{Y}$ was a maximum] .* It was found that

$$\tau_g = 0.31$$

this corresponds to a dimensional time $t = t_g$, then;

$$t_g = 0.31\ \alpha^{-1} \quad . \tag{67}$$

It might be noted that negligible transfer of excitation occurred for $\delta f > 10\ \alpha$. [The arbitray choice $|\delta f| \leq \alpha$ used in evaluating α is of course compensated in the numerical value for τ_g, since t_g is independent of this choice.]

Our dimensionless scaling of Eqs. (59) was of course motivated by the simple model calculation of the last section. It is interesting to note that our elaborate numerical calculation was very close to the predictions of this model based on the locked phase and parametric amplifier approximations.

To evaluate t_g, using Eqs. (66) and (67) the Garrett-Munk ocean model [Eq. (2)] and the WKB approximation were used. The resulting values of the growth time are shown in Figs. (8) - (11) for a range of parameters.

In Fig. (8) we show t_g (in seconds) as a function of

---

*For Y well below its saturation value the choice of time at which to evaluate τ_g was not very critical.

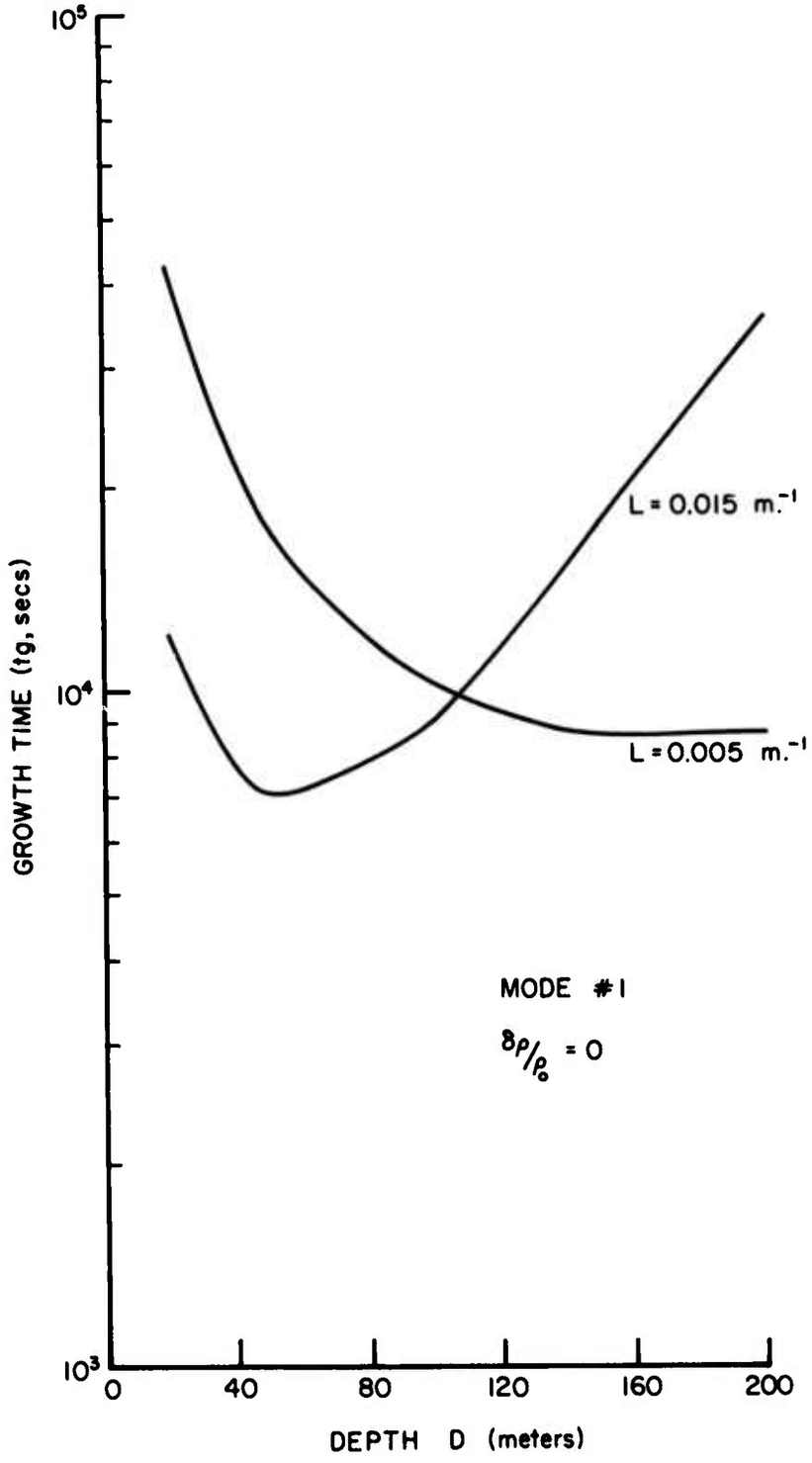
10^5
10^4
10^3
GROWTH TIME (tg, secs)
L = 0.015 m.$^{-1}$
L = 0.005 m.$^{-1}$
MODE #1
$\delta\rho/\rho_0 = 0$
0
40
80
120
160
200
DEPTH D (meters)

XBL 752-276

the mixed layer thickness D for the modes j = 1, L = 0.015 and 0.005 m^{-1} and with $\delta\rho/\rho_o = 0$.

In fig. (9) we show t_g as a function of $\delta\rho/\rho_o$ for D = 100 m, L = 0.01 m^{-1}, and j = 1,2,3.

Finally, in Figs. (10) and (11) we show t_g as a function of L for j = 1,2,3, D = 100 m, and $\delta\rho/\rho_o = 0, 10^{-3}$.

The weak excitation of the high order modes is a consequence of their extending to greater depths. This greater depth increases the value of g'(j,L) [Eq. (28)] and thus reduces the coupling strength [This is seen, for example, in Eq. (66)]. The very weak coupling between surface and internal waves found by Kenyon (1968) is related to this observation. Kenyon used a constant thermocline model, for which the internal wave extends to the bottom, leading to a very large g'(j,L) for all modes. Since the coupling interaction occurs near the ocean surface, the deeper the internal wave extends, the less effective coupling appears to be. Our conclusions are consistent with those of Joyce (1974), who noted that his two layer model gave much stronger coupling than that found by Kenyon.

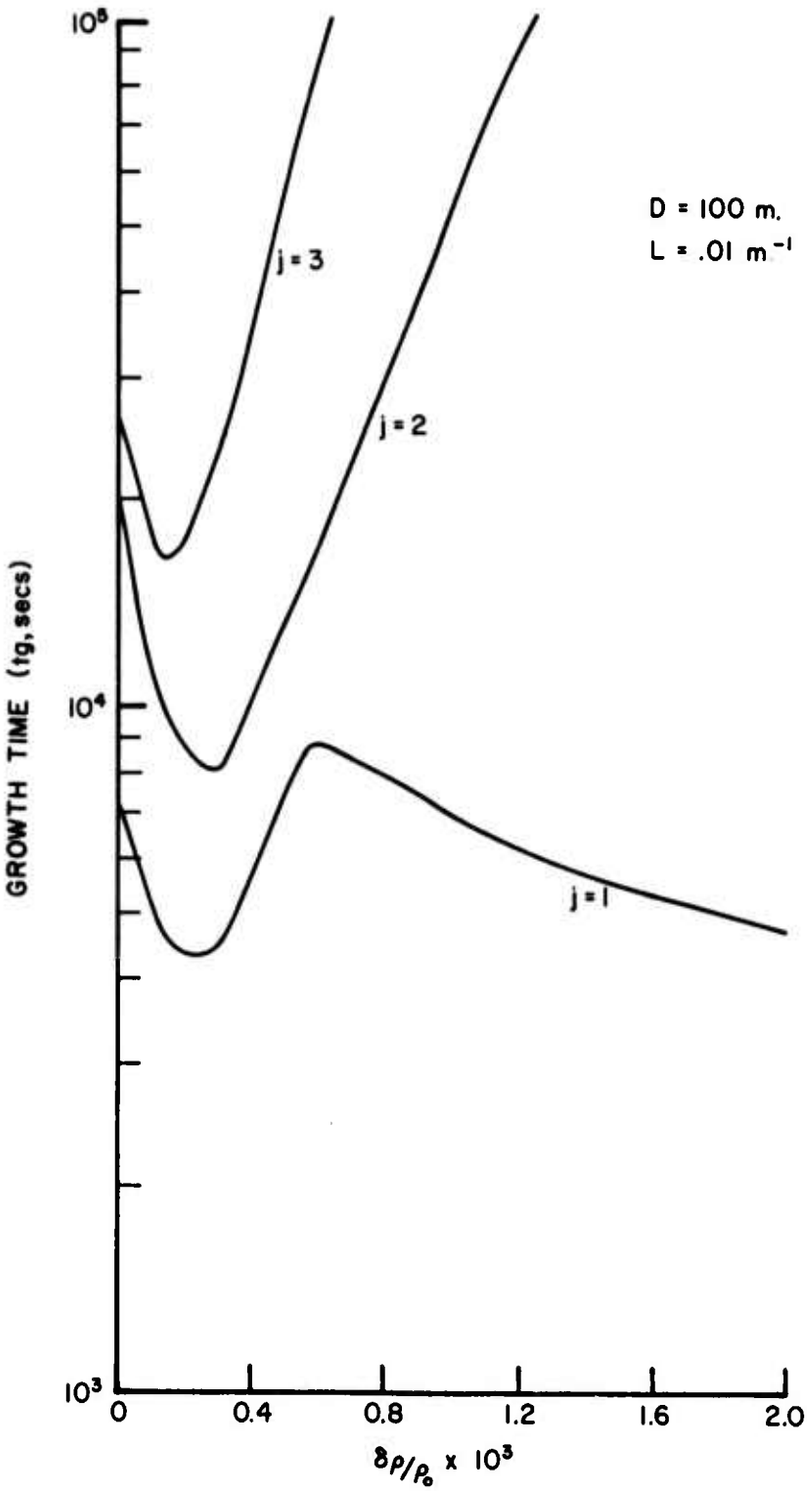
10^5
10^4
10^3
GROWTH TIME (tg, secs)
D = 100 m.
L = .01 m^{-1}
j = 3
j = 2
j = 1
0
0.4
0.8
1.2
1.6
2.0
$\delta\rho/\rho_0 \times 10^3$

XBL 752-275

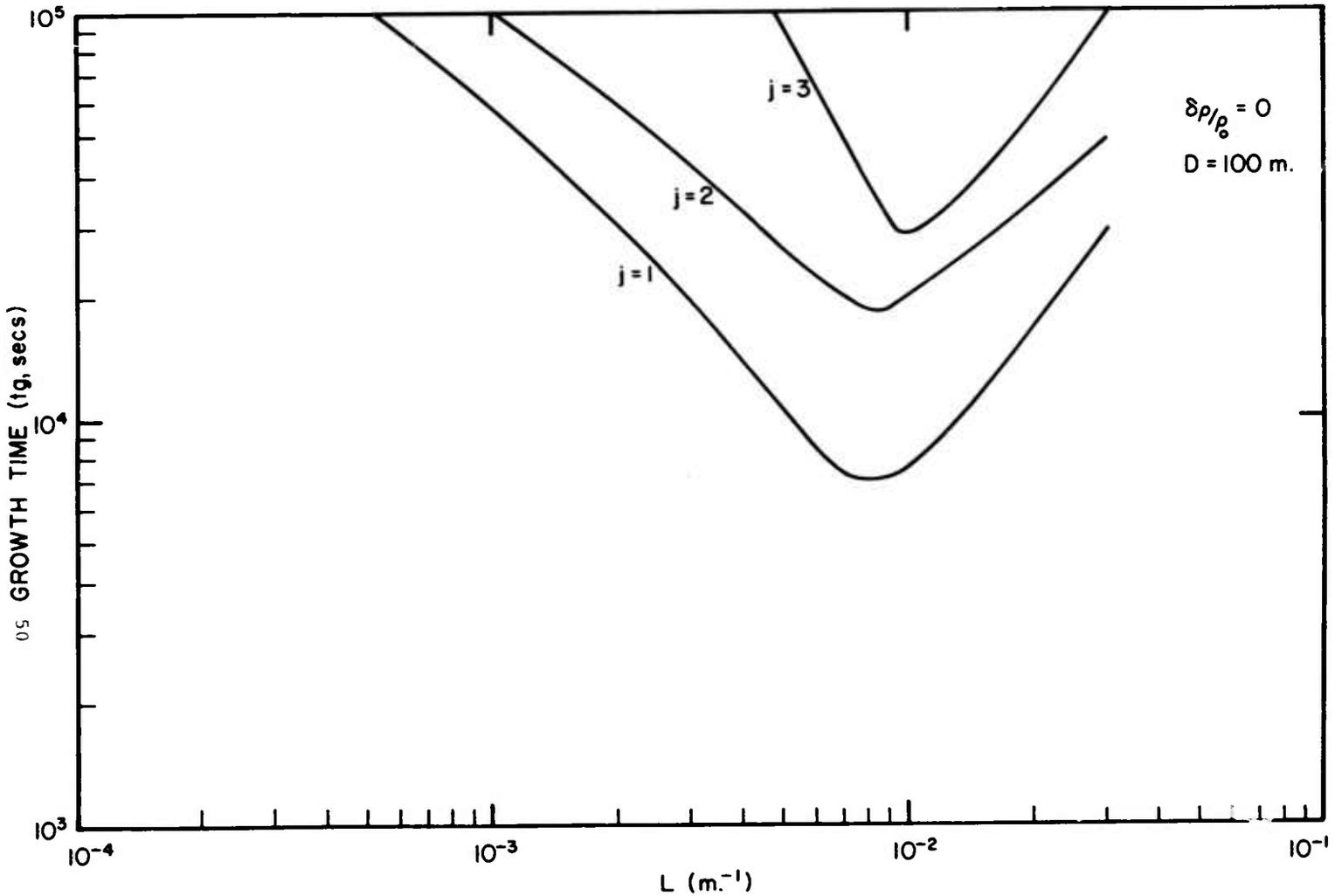
10^5
10^4
10^3
GROWTH TIME (tg, secs)
j = 3
j = 2
j = 1
$\delta\rho/\rho_0 = 0$
D = 100 m.
10^{-4}
10^{-3}
10^{-2}
10^{-1}
L ($m.^{-1}$)

XBL 752-279

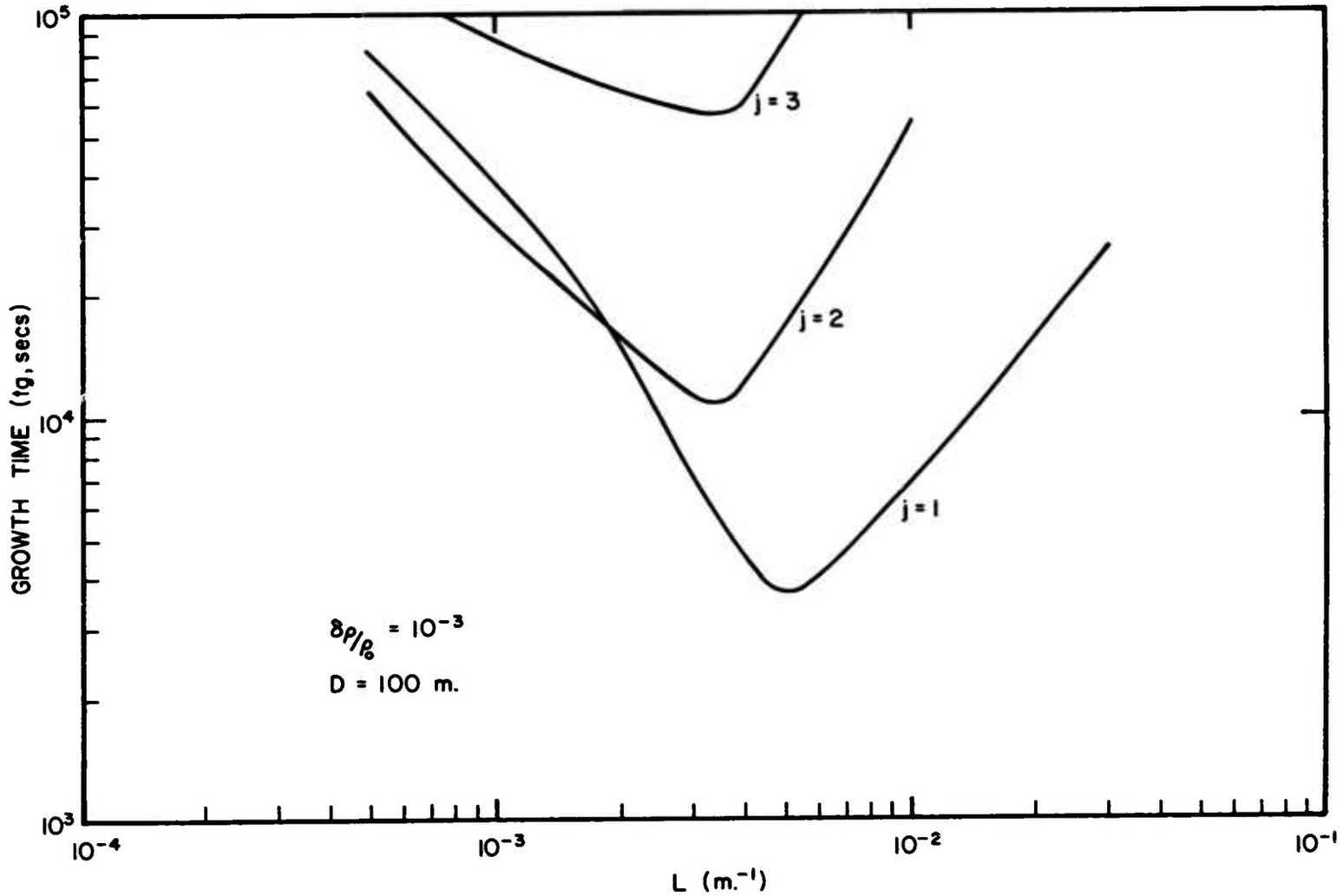
GROWTH TIME (tg, secs)
10^5
10^4
10^3
10^{-4}
10^{-3}
10^{-2}
10^{-1}
L ($m.^{-1}$)
j = 3
j = 2
j = 1
$\delta\rho/\rho_o = 10^{-3}$
D = 100 m.

XBL 752-278

VI. VISIBILITY OF INTERNAL WAVES ON OCEAN SURFACE

In the preceeding sections the growth of an internal wave was examined under a variety of oceanographic conditions and the growth rate calculated as a function of the environmental parameters. Our attention was focused on the energy transfer from surface to internal waves via the resonant triad interaction and the modification of the surface wave spectrum was not discussed. In this section we examine this modulation of the surface wave spectrum by the internal wave and discuss the "visibility" of the internal waves from such surface modifications.

The modulation of the surface wave spectrum induced by travelling internal waves is visible to both the eye and radar (Ziegenbein, 1970; Perry and Schimke, 1965; Gargett and Hughes, 1972). Lafond (1962) suggested that the internal wave redistributes extant organic material on the ocean surface leading to variable slope and reflectivity properties of the surface which are phase correlated with the internal wave. Gargett and Hughes (1972) brought this interpretation into question by noting the directional preference of the surface wave modifications visible in the Straits of Georgia, i.e., the surface gravity waves have long crests parallel to the internal waves. Such a phenomenon is inconsistent with a surface-film mechanism for producing "slicks," but not with a direct mechanical interaction such as surface wave scattering from the surface currents produced by the internal wave.

The analyses of the mechanical interaction between surface and internal waves Ball (1961); Gargett and Hughes (1972); Nesterov (1972); Lewis et al. (1974) and Thomson and West (1975) assume the internal wave to be of sufficiently large amplitude that the energy transfer is from the internal to the surface waves, i.e., no internal wave generation.

To examine the modulation of the surface wave spectrum induced by an evolving internal wave spectrum, using a numerical integration of the Hamiltonian equations, we consider the two model systems shown in Table II. In the first system we include the four surface modes $\underset{\sim}{k}_i$ (i = 1, 2, 3, 4) with amplitudes determined from Eq. (45). The four internal modes $\underset{\sim}{L}_i$ (i = 1, 2, 3, 4) have zero initial amplitude.

In Figure 12 the rms amplitude of the internal wave modes are depicted. Only mode $\underset{\sim}{L}_1$ and $\underset{\sim}{L}_4$ have the appropriate wave vectors to grow significantly in this time interval (approximately 5.5 hours) by the resonant triad interaction with the surface wave spectrum selected. The linear approximation to the internal wave dispersion relation is tested by doing the calculation twice. There is no appreciable effect in the lowest mode $\underset{\sim}{L}_1$, but the second harmonic changes significantly. The bumps in the growth curve are due to frequency mismatch induced by the nonlinear coupling.

The two dimensional view of the ocean surface looking down from above is shown in Figure 13 where contours of equal

TABLE II

Wave Vectors	I	II
$\underset{\sim}{k}_1$	$(.03\ m^{-1}, 0°)$	$(.0298\ m^{-1}, \Theta_n)$
$\underset{\sim}{k}_2$	$(.029887\ m^{-1}, -1.9°)$	$(.030\ m^{-1}, \Theta_n)$
$\underset{\sim}{k}_3$	$(.029816\ m^{-1}, -3.8°)$	$(.0302\ m^{-1}, \Theta_n)$
$\underset{\sim}{k}_4$	$(.029779, -5.7°)$	$(.0304\ m^{-1}, \Theta_n)$
$\underset{\sim}{L}_1$	$(10^{-3}m^{-1}, 83°)$	$(4\times10^{-4}m^{-1}, 90°)$, $(4.47\times10^{-4}m^{-1}, 63.4°)$
$\underset{\sim}{L}_2$	$(1.988\times10^{-3}m^{-1}, 86.5°)$	$(6\times10^{-4}m^{-1}, 90°)$, $(6.32\times10^{-4}m^{-1}, 71.6°)$
$\underset{\sim}{L}_3$	$(1.021\times10^{-3}m^{-1}, 76.3°)$	$(8\times10^{-4}m^{-1}, 90°)$, $(8.2\times10^{-4}m^{-1}, 78°)$
$\underset{\sim}{L}_4$	$(2\times10^{-3}m^{-1}, 83°)$	$(10^{-3}m^{-1}, 90°)$, $(1.02\times10^{-3}m^{-1}, 78.7°)$
$\underset{\sim}{L}_5$	----------	$(1.2\times10^{-3}m^{-1}, 90°)$, $(1.217\times10^{-3}m^{-1}, 80.5°)$

In column I the wavevectors for four surface modes $\underset{\sim}{k}_1$, ..., $\underset{\sim}{k}_4$ and four internal modes $\underset{\sim}{L}_1$, ..., $\underset{\sim}{L}_4$ are listed in polar coordinates. In column II the wave vectors for twenty four surface modes are listed, where for each wavenumber (k) there are six angles given by $\Theta_n = -.38°n$, $n = 0, 1, \ldots, 5$. Also in column II are listed ten internal modes in polar coordinates.

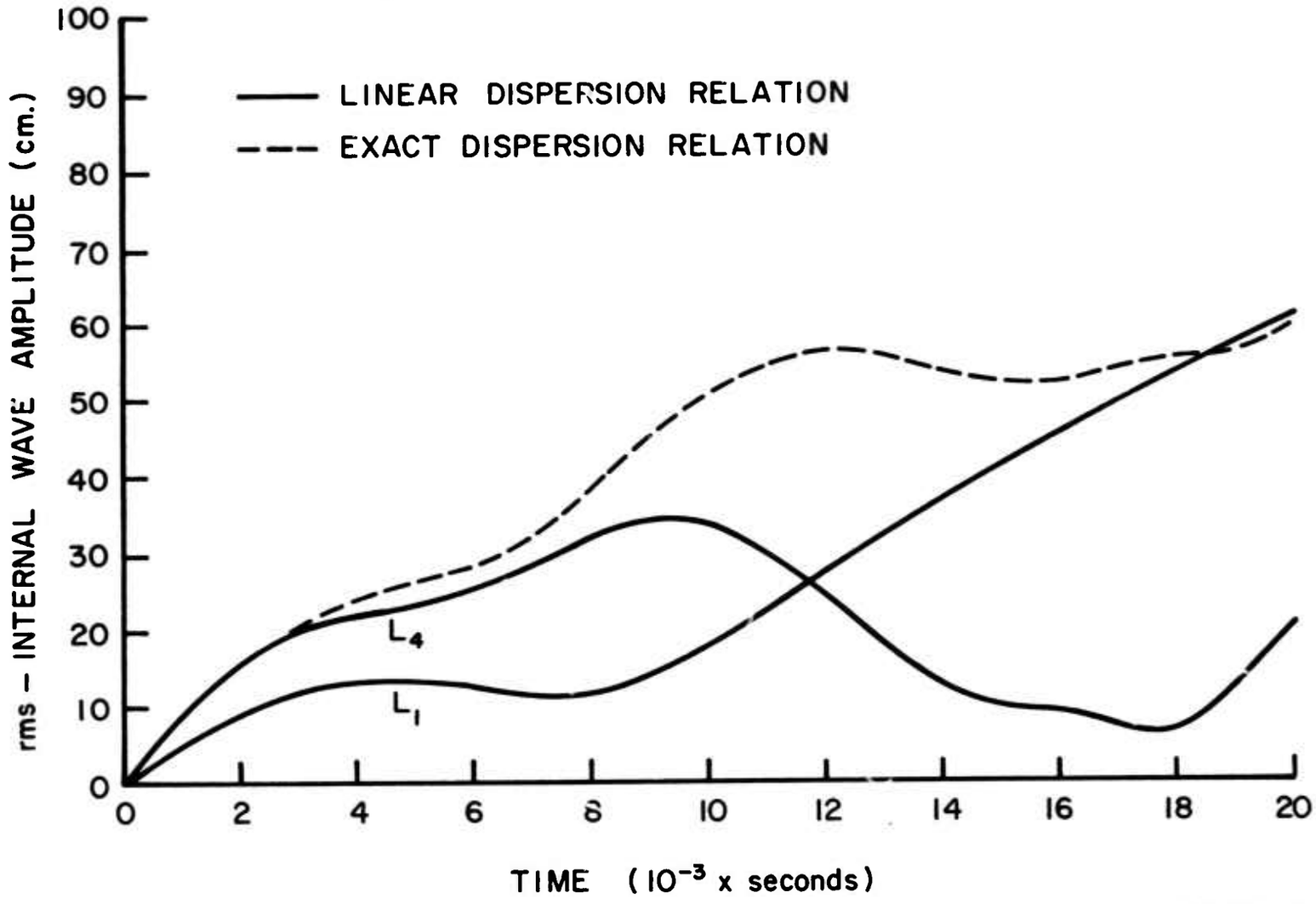
LINEAR DISPERSION RELATION
EXACT DISPERSION RELATION
rms – INTERNAL WAVE AMPLITUDE (cm.)
100
90
80
70
60
50
40
30
20
10
0
0
2
4
6
8
10
12
14
16
18
20
L_4
L_1
TIME (10^{-3} x seconds)

XBL 752-191

surface height are shown. From column I of Table II we see that the surface waves are travelling in a narrow cone from left to right and from Figure 13 they produce a weak interference pattern in approximately the y direction at time t = 0. In Figure 14 the negligible initial amplitude of the internal wave field is shown as contours of equal height, along with the direction of the modes included in the calculation.

Figure 15 depicts contours of equal surface slope (in magnitude) at time t = 0, ie., $|\nabla\zeta(\underset{\sim}{x},t)|$. The intensity of incoherent light backscattered from the ocean surface is dependent on the mean square surface slope. By averaging the slope contours in Figure 15 over a length large compared to the surface wavelengths, and small compared to the internal wavelength, one obtains a measure of the 'visibility' of the surface modulation pattern.

After 2×10^4 sec the internal wave has developed to an amplitude of 1.44 m. The contours of equal height are a series of ridges as shown in Figure 16. In Figure 17 the correlation of the surface wave modulation pattern with the internal wave amplitude is clearly seen. The small scale structure in Figures (15) and (17) is the "mottling" discussed by Apel et al. (1975a) and arises from the self interference of the surface waves. This effect is enhanced by the growth of the internal wave.

An observation of this long wavelength modification in the surface wave structure (approximately .6 km) was reported

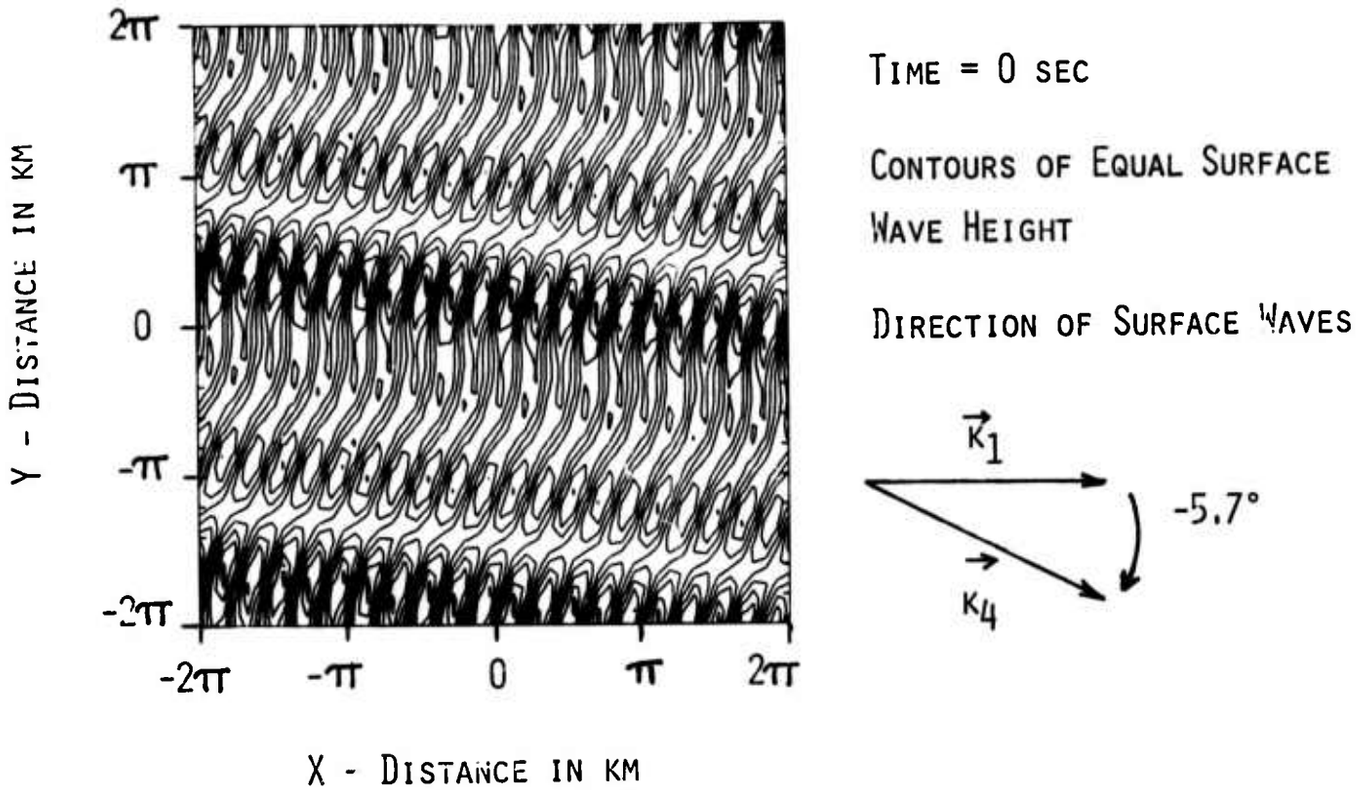
2π
π
0
-π
-2π
-2π
-π
0
π
2π
Y - DISTANCE IN KM
X - DISTANCE IN KM
TIME = 0 SEC
CONTOURS OF EQUAL SURFACE WAVE HEIGHT
DIRECTION OF SURFACE WAVES
$\vec{K}_1$
-5.7°
$\vec{K}_4$

Figure 13

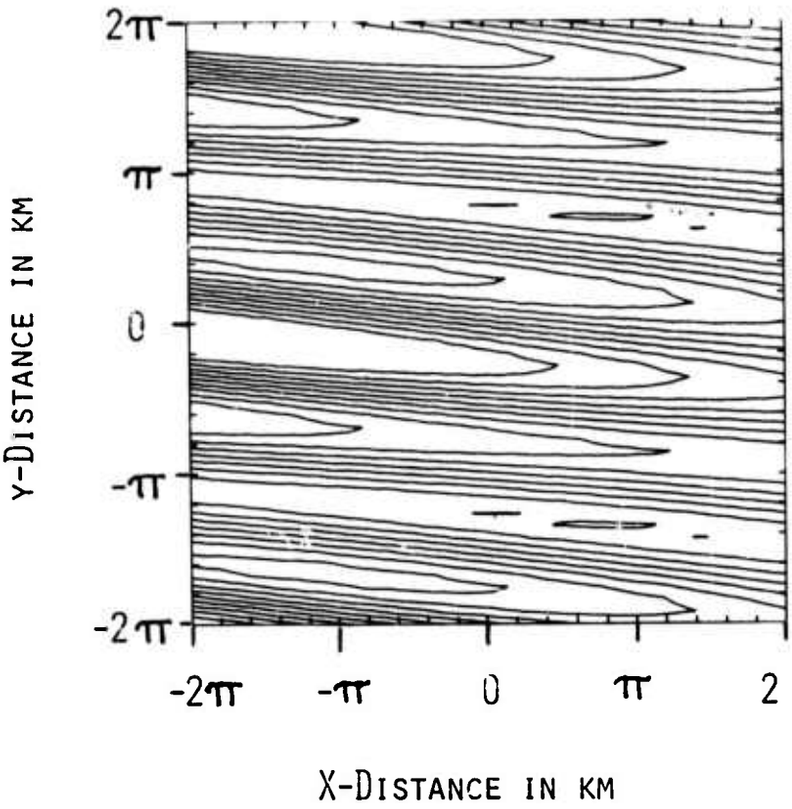

TIME = 0 SEC.

CONTOURS OF EQUAL INTERNAL WAVE HEIGHT

DIRECTION OF INTERNAL WAVES

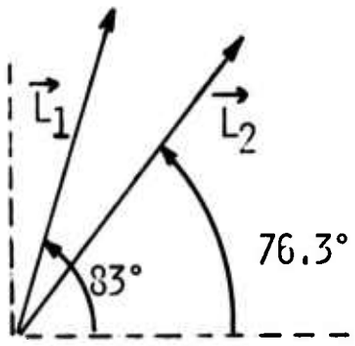

Figure 14

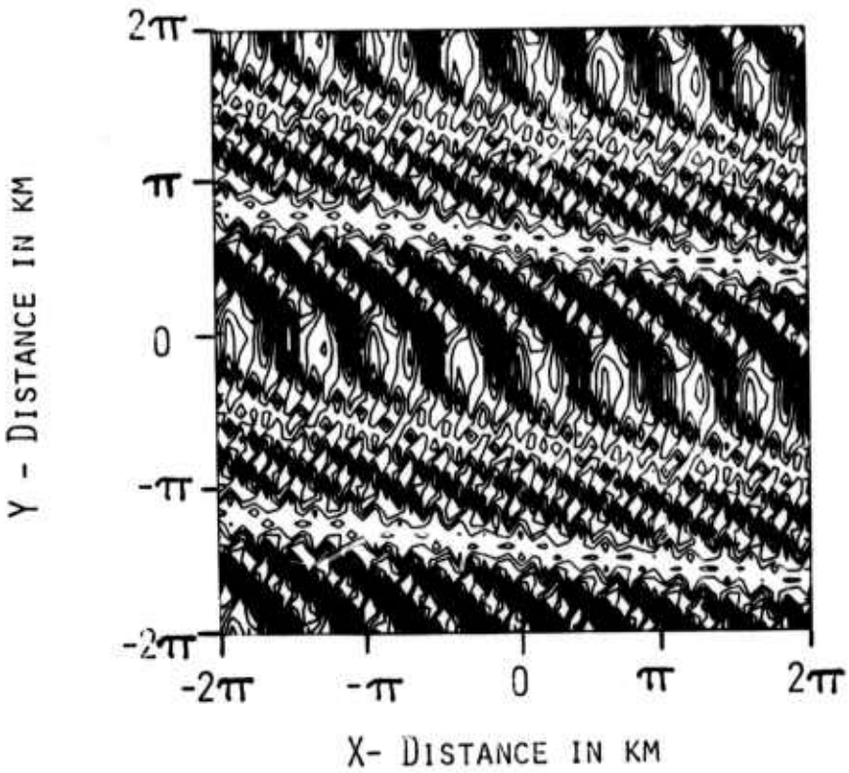

TIME = 0 SEC

CONTOURS OF EQUAL MAGNITUDE OF SURFACE SLOPE

Figure 15

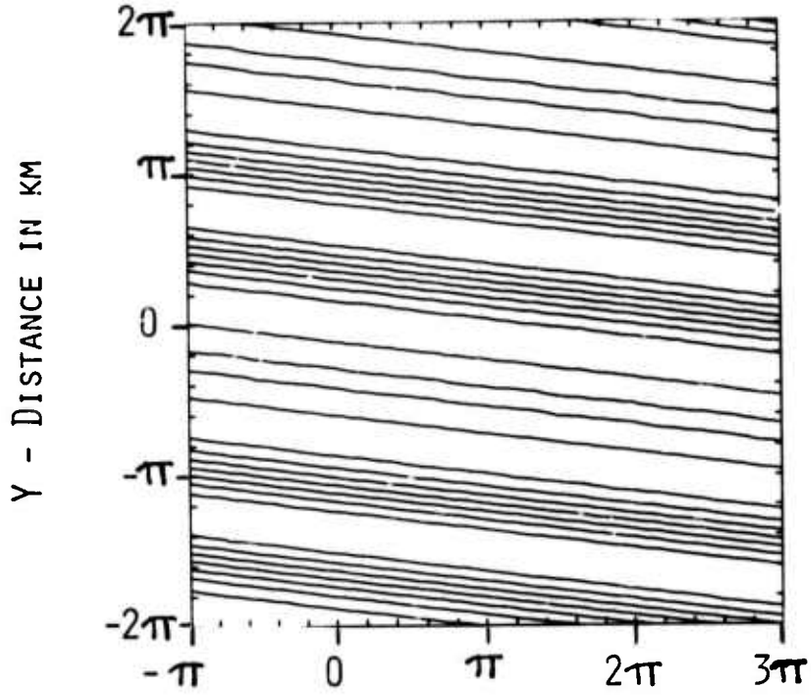

TIME = 2×10^4 SEC.

CONTOURS OF EQUAL INTERNAL WAVE HEIGHT

MAXIMUM HEIGHT 1.44 M

Figure 16

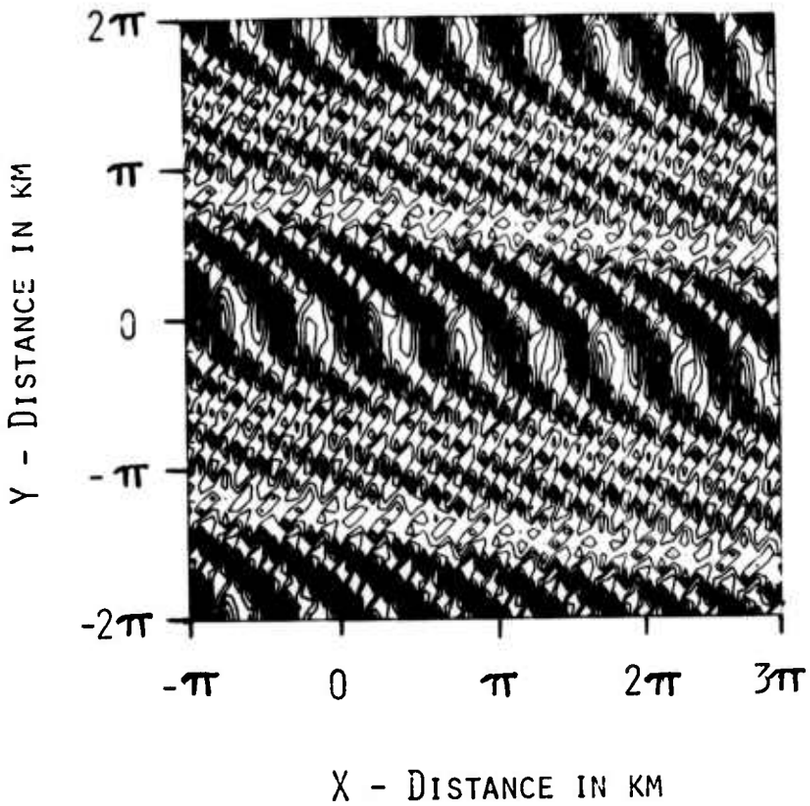
2π
π
0
-π
-2π
-π
0
π
2π
3π
Y - DISTANCE IN KM
X - DISTANCE IN KM
TIME = 2x10^4 SEC
CONTOURS OF EQUAL MAGNITUDE OF SURFACE SLOPE

Figure 17

by Apel et al. (1975b) in discussing pictures of the ocean surface obtained from the ERTS satellite. This is the order of one small scale division in Figures (13) - (17). The internal waves were assumed to be generated by tidal currents impinging on the continental shelf and the interaction with surface waves produced the visible surface patterns.

A final example uses a total of 24 surface and 10 internal modes as listed in Column II of Table II to represent the ocean environment. In this case, in addition to the surface waves having the equilibrium amplitudes prescribed by Eq. (45), the internal waves amplitudes are given by the Garrett and Munk (1972a) spectrum Eq. (47). The resulting initial surface pattern (contours of equal height) is shown in Figure 18. The corresponding contours for the internal wave field are shown in Figure 19.

The response of the ocean surface to this internal wave spectrum is depicted in Figure 20, where contours of equal wave slope (magnitude) are shown. The surface shown in Figure 20 is again qualitatively similar to the "mottling" of the ocean surface observed in photographs taken from the ERTS satellite. [Apel (1975a)].

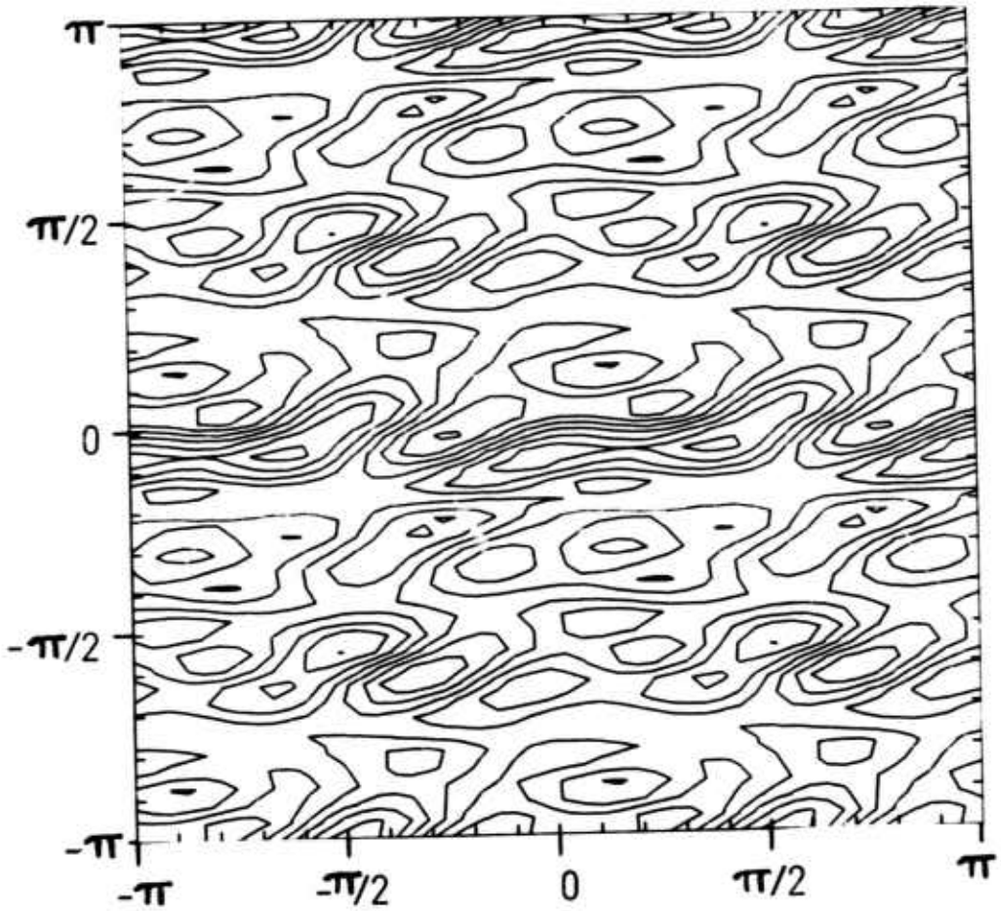

Time = 0 sec

Contours of Equal Surface Wave Height

Maximum Height 21.5 m

Direction of Surface Waves

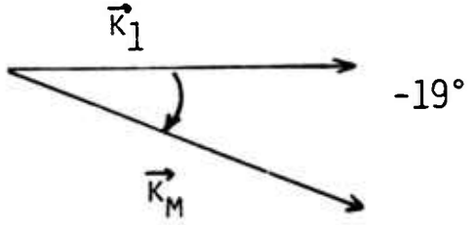

Figure 18

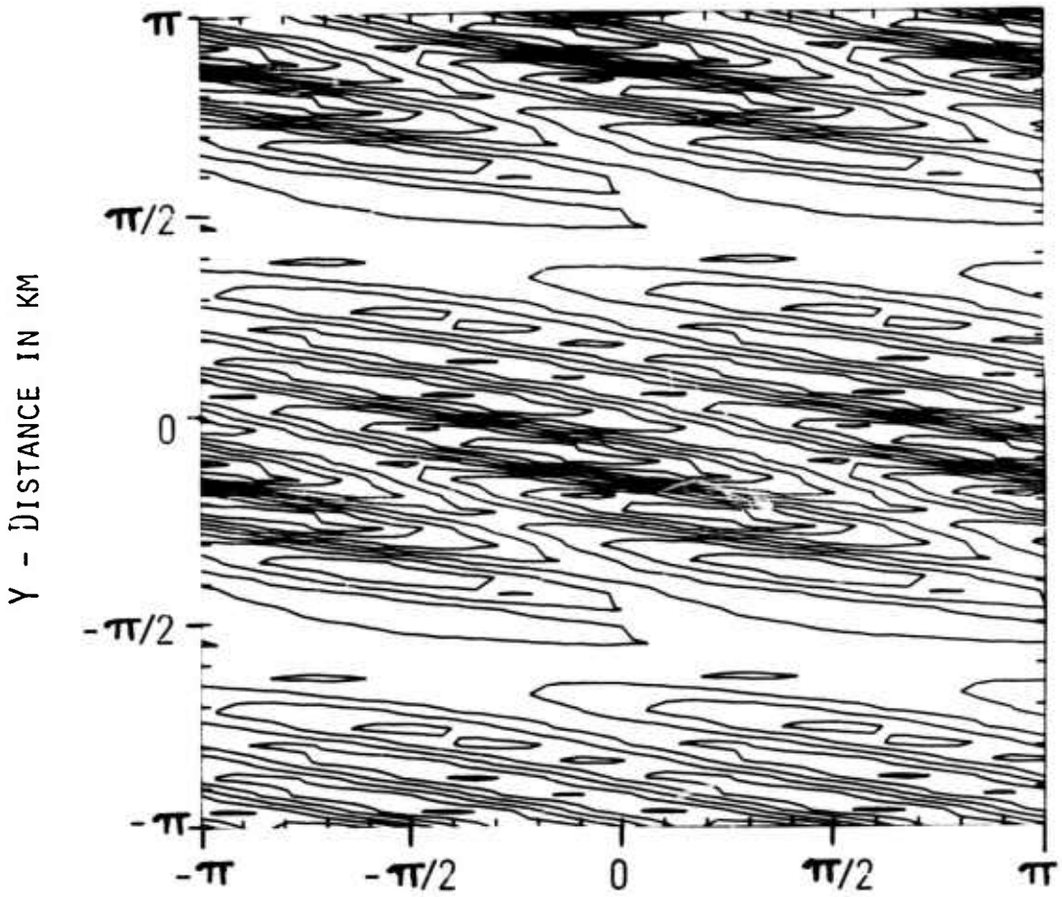

TIME = 0 SEC

CONTOURS OF EQUAL INTERNAL WAVE HEIGHT

MAXIMUM HEIGHT = 3.2 M

DIRECTION OF INTERNAL WAVES

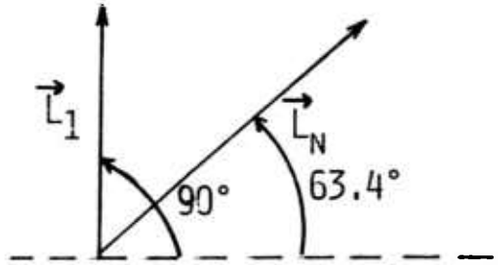

Figure 19

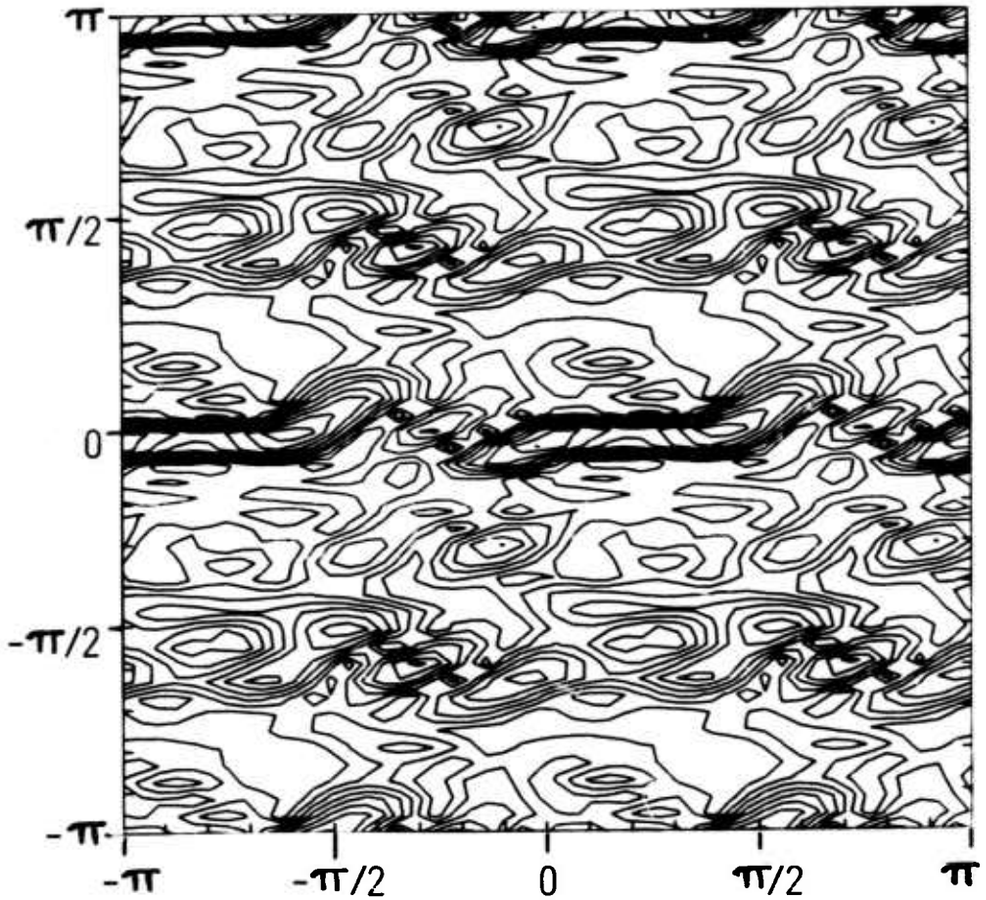

Time = 200 sec

Contours of Equal Magnitude of Surface Slope

Maximum Slope = .69
(initially .61)

Figure 20

VII. DISCUSSION AND CONCLUSIONS

The intent of this paper has been to present a theoretical model with which the energy exchange between ocean surface waves and internal waves can be calculated. The Hamiltonian model is, of course, limited in its description of the energy transfer process in an oceanographic environment. The nonlinear interactions among surface waves, as well as, among internal waves have not been included in the model. Also, the coupling of the wind to the air-sea interface has been ignored. On the long time scale of the surface-internal wave interaction (characteristically several hours) these phenomena can significantly influence developing surface and internal wave spectra. However, in the equilibrium case, when the generation and dissipation (or transfer) rates of surface waves are in balance, the general conclusions based on the analysis and calculations are thought to be useful.

The calculated interaction times given in Figs. (10) and (11) can be used to estimate the rate at which energy is fed to the internal wave system by surface waves. The second of the relations (44) lets us write the power per unit area delivered to the internal waves of mode number j as

$$P_j = \rho_o \int g'(j,L)\ \Psi_I(j,L)\ d^2L/t_g \quad .$$

We have evaluated this integral using the Garrett-Munk spectrum (47) and t_g taken from Fig. (10). The integration was

restricted to the range $L > 7\times10^{-4}m^{-1}$, since Fig. (3) (and our numerical calculations) suggest that when $L > 7\times10^{-4}m^{-1}$ the internal wave energy per mode is too large to receive substantial energy from the surface waves. The results for j = 1, 2 were

$$P_1 \simeq 3 \text{ ergs/cm}^2\text{/sec}$$

$$P_2 \simeq \frac{1}{2} \text{ erg/cm}^2\text{/sec} \quad ,$$

the principal contribution coming from the range

$$7\times10^{-4}m^{-1} < L < 5\times10^{-3}m^{-1} \quad .$$

These transfer rates are surprisingly close to the value of about 1 erg/cm^2/sec obtained by Bell (1975) from considerations of internal tides. They are also not very dissimilar from the dissipation rate of approximately 7 ergs/cm^2/sec estimated by Garrett and Munk (1972b).

REFERENCES

Apel, J.R., Byrne, H.M., Proni, J.R. and Charnell, R.L., 1975a J. Geophys. Res. 80, 865.

Apel, J.R., Proni, J.R., Byrne, H.M., and Sellers, R.L. 1975b, to appear in Geophys. Res. L ett.

Ball, F.K. 1964 J. Fluid Mech. 19, 465.

Bell, T.H. 1975 J. Geophys. Res. 80, 320.

Cohen, B.I., Kaufman, A.N., and Watson, K.M. 1972 Phys. Rev. Letters 29, 581.

Gargett, A.E. & Hughes, B.A. 1972 J. Fluid Mech. 52, 179.

Garrett, C. & Munk, W. 1972a Geophys. Fluid Dyn. 2, 179.
1972b Deep Sea Res. 19, 823.
1975 J. Geophys. Res. 19, 291.

Joyce, T.M. 1974 J. Fluid Mech. 63, 801.

Kenyon, K. 1968 J. Marine Res. 26, 208.

Lafond, E.C. 1962 in The Sea 1, Publ. by Interscience Publishers, John Wiley and Sons, 731.

Lewis, J.E., Lake, B.M. & Ko, D.R.S. 1974 J. Fluid Mech. 63, 773.

Nesterov, S.U. 1972 Atmos. and Oceanic Phys. 8, 447.

Nishikawa, K. 1968 J. Phys. Soc. of Japan 24, 916.

Perry, R.B. & Schimke, G.R. 1965 J. Geophys. Res. 70, 2319.

Phillips, O.M. 1966 The Dynamics of the Upper Ocean Cambridge University Press.

Sturrock, P.A., 1960 Annals of Phys. 9, 422.

Thorpe, S.A. 1975 J. Geophys. Res. 80, 328.

Thomson, J.A.L. & West, B.J. 1975 to appear in J. Phys. Oceanography.

Tyler, G.L., Teague, C.C., Steward, R.H., Peterson, A.M., Munk, W. Joy, J.W. 1974 Deep Sea Res. 21, 989.

Ziegenbein, J. 1970 Deep Sea Res. 17, 867.

ACKNOWLEDGMENT

The authors would like to thank Dr. Walter Munk for several discussions and comments concerning this work. They would also like to thank Dr. John Apel for both correspondence and discussions concerning the ERTS satellite observations.

This research was partially supported by the Defense Advanced Research Projects Agency (DARPA), 1400 Wilson Boulevard, Arlington, VA 22209, and monitored by the Air Force Systems Command, Rome Air Development Center, Griffiss Air Force Base, New York 13440, under Contract F30602-72-C-0494.

APPENDIX THE HAMILTONIAN

In this Appendix we discuss the Hamiltonian (35) in more detail than was given in Section II. That Eq. (35) is the correct Hamiltonian may be verified by simply observing that the equations of motion (38) are equivalent to Eqs. (12), (30), and (31).

It is also easily verified that the energy associated with the surface waves is

$$\hat{H}_s = \frac{\rho_o}{2} \int d^2r \left[\left(\circledast^{1/2} \phi_s \right)^2 + g\zeta^2 \right] \tag{A.1}$$

Canoncial variables may be introduced with the relations

$$Q(\underset{\sim}{r}) = \sqrt{\frac{\rho}{g}} \quad \phi_s(\underset{\sim}{r}) \quad ,$$

$$\Pi(\underset{\sim}{r}) = - (\rho_o g)^{\dot{1}/2} \quad \zeta(\underset{\sim}{r}) \quad , \tag{A.2}$$

so

$$\hat{H}_s = \frac{1}{2} \int d^2r \left[\Pi^2 + g \left(\circledast^{1/2} Q \right)^2 \right] . \tag{A.3}$$

The equations of motion are

$$\dot{\Pi}(\underset{\sim}{r}) = - \frac{\delta \hat{H}_s}{\delta Q(\underset{\sim}{r})} = -g \circledast Q(\underset{\sim}{r}) \quad ,$$

$$Q(\underset{\sim}{r}) = \frac{\delta \hat{H}_s}{\delta \pi(\underset{\sim}{r})} = \Pi(\underset{\sim}{r}) \quad , \tag{A.4}$$

which are equivalent to the linearized surface wave equations. Finally, the Hamiltonian per unit area of Eqs. (35) and (36) is

$$H_s = \hat{H}_s / A_o \quad .$$

Use of Eqs. (32) and (A.4) gives the form (36) of H_s.

The internal wave energy is a little more involved obtain. We can calculate the gravitational potential energy as follows. Let the displacement of a fluid element be given by two steps. The first is a vertical displacement $S(z,\underset{\sim}{r},t)$. The second is a horizontal displacement to give the actual flow. The second step does not change the gravitational energy, so we need study only the first (virtual) displacement S.

The density following the displacement S is

$$\rho(\underset{\sim}{x}) = \bar{\rho}(z-S)\left(1 - \frac{\partial S}{\partial z}\right) . \tag{A.5}$$

The potential energy is then

$$PE = g \int d^2r \int_{-H}^{0} dz \quad z\left[\rho(\underset{\sim}{x}) - \bar{\rho}(z)\right] .$$

Using Eq. (A.5) and expanding to second order in S, we finally obtain

$$PE = \frac{\rho_o}{2} \int d^2r \int_{-H}^{0} N^2 S^2 \, dz \quad . \tag{A.6}$$

Now, using Eq. (20), we have

$$\frac{\partial S}{\partial t} = w = \sum_{j,\underset{\sim}{L}} W_{j,\underset{\sim}{L}} A_{j,\underset{\sim}{L}} \exp(i\underset{\sim}{L}\cdot\underset{\sim}{r}) \quad ,$$

or

$$S = \sum_{j,\underset{\sim}{L}} B_{j,L} W_{j,\underset{\sim}{L}} \exp(i\underset{\sim}{L}\cdot\underset{\sim}{r}) \quad ,$$

where

$$\dot{B}_{j,\underset{\sim}{L}} = A_{j,\underset{\sim}{L}} \quad .$$

This permits us to write

$$PE = \sum_{j,\underset{\sim}{L}} \frac{\rho_o}{2} \int d^2r \int_{-H}^{0} N^2 W^2_{j,\underset{\sim}{L}}(z) \, dz \, B^2_{j,\underset{\sim}{L}}$$

$$= \sum_{j,\underset{\sim}{L}} \frac{\rho_o}{2} \int d^2r \; g'(j,L) \; W^2_{j,\underset{\sim}{L}} \; (-D) \; B^2_{j,\underset{\sim}{L}}$$

$$= \frac{\rho_o}{2} \sum_{j=1} \int d^2r \; g'(j,\textcircled{\#}) \; \xi^2_j(\underset{\sim}{r},t) \quad , \tag{A.7}$$

using Eq. (28) and the relation $S(-D,\underset{\sim}{r},t) = \sum_{j=1} \xi_j(\underset{\sim}{r},t)$,

The internal wave kinetic energy is

$$KE = \frac{\rho_o}{2} \int d^2r \int_{-H}^{0} dz \left[w^2 + \underset{\sim}{q}^2 \right] \quad , \tag{A.8}$$

where $\underset{\sim}{q}$ represents the horizontal components of the fluid velocity. Use of the condition

$$\frac{\partial w}{\partial z} + \nabla_s \cdot \underset{\sim}{q} = 0$$

and Eq. (7) allows simplification to the form

$$KE = \frac{\rho_o}{2} \sum_{j=1} \int d^2r \left[g'(j,\#) \ \#^2 \ \sinh^2(D\#)/\Omega^2(j,\#) \right] \Phi_j(\underset{\sim}{r}) \tag{A.9}$$

Finally, canonical variables are introduced with the relations

$$Q_I(\underset{\sim}{r}) = \rho_o^{1/2} \ \Omega^{-1} \ T \ \Phi_j(\underset{\sim}{r}) \quad ,$$

$$\Pi_I(\underset{\sim}{r}) = (\rho_o g')^{1/2} \ \xi_j(\underset{\sim}{r},t) \tag{A.10}$$

and

$$\hat{H}_I \equiv A_o \ H_I = \frac{1}{2} \sum_{j=1}^{\infty} \int d^2r \left[\Pi_I^2 + \left(\Omega Q_I \right)^2 \right] \quad . \tag{A.11}$$

where the j dependence of Q_I and Π_I is implicit.
The resulting Hamiltonian equations of motion are seen to describe internal waves in the linear approximation.

The interaction V in Eqs. (35) and (36) is:

$$V = A_o^{-1}\,\hat{V} = -A_o^{-1}\sum_{j=1}\int d^2r\;\; \Pi(\nabla_s Q)\cdot\left[\rho_o^{-1/2}\Omega T^{-1}\nabla_s Q_I\right] \quad . \qquad (A.12)$$

The set of Eqs. (12), (30), and (31) are equivalent to the set of Hamiltonian equations

$$\hat{H} = \hat{H}_s + \hat{H}_I + \hat{V} \quad ,$$

$$\dot{Q}(\underset{\sim}{r}) = \frac{\delta \hat{H}}{\delta \Pi(\underset{\sim}{r})} \quad , \quad \dot{Q}_I(r) = \frac{\delta \hat{H}}{\delta \Pi_I(\underset{\sim}{r})} \quad , \ldots \quad . \qquad (A.13)$$

We also have the Poisson bracket relations

$$\left[Q(\underset{\sim}{x}) \;,\; \Pi(\underset{\sim}{y})\right] = \delta(\underset{\sim}{x}-\underset{\sim}{y}) \quad , \text{ etc.}$$

The above field variables may be Fourier expanded over the unit area A_o as follows:

$$Q(\underset{\sim}{r}) = \sum_{\underset{\sim}{k}} \left[C_{\underset{\sim}{k}}\, q_{\underset{\sim}{k}} - \omega_k^{-1}\, S_{\underset{\sim}{k}}\, p_{\underset{\sim}{k}}\right]\Big/\sqrt{2} \quad ,$$

$$\Pi(\underset{\sim}{r}) = \sum_{\underset{\sim}{k}} \left[C_{\underset{\sim}{k}}\, p_{\underset{\sim}{k}} + \omega_k\, S_{\underset{\sim}{k}}\, q_{\underset{\sim}{k}}\right]\Big/\sqrt{2} \quad ,$$

$$Q_I(\underset{\sim}{r}) = \sum_{j,\underset{\sim}{L}} \left[C_{\underset{\sim}{L}}\, Q(j,\underset{\sim}{L}) - \Omega^{-1}(j,L) S_{\underset{\sim}{L}} P(j,\underset{\sim}{L})\right]\Big/\sqrt{2} \quad ,$$

$$\Pi_I(\underset{\sim}{r}) = \sum_{j,\underset{\sim}{L}} \left[C_{\underset{\sim}{L}}\, P(j,\underset{\sim}{L}) + \Omega(j,L) S_{\underset{\sim}{L}}\, Q(j,\underset{\sim}{L})\right]\Big/\sqrt{2} \quad , \qquad (A.14)$$

where

$$S_{\underset{\sim}{k}} = (2/A_o)^{1/2} \sin \underset{\sim}{k} \cdot \underset{\sim}{r} \quad ,$$

$$C_{\underset{\sim}{k}} = (2/A_o)^{1/2} \cos \underset{\sim}{k} \cdot \underset{\sim}{r} \quad .$$

The transformation from the Q, Π, etc. to the $q_{\underset{\sim}{k}}$, $p_{\underset{\sim}{k}}$ is a canonical transformation, the Poisson bracket relations for the new variables being

$$\left[q_{\underset{\sim}{k}} , p_{\underset{\sim}{k}} \right] = \delta_{\underset{\sim}{k},\underset{\sim}{k}'}, \qquad \text{etc.}$$

We also have

$$\hat{H}_s = \frac{1}{2} \sum_{\underset{\sim}{k}} \left(p_{\underset{\sim}{k}}^2 + \omega_k^2 \, q_{\underset{\sim}{k}}^2 \right) \quad ,$$

$$\hat{H}_I = \frac{1}{2} \sum_{j,\underset{\sim}{L}} \left[P^2(j,\underset{\sim}{L}) + \Omega^2(j,L) Q^2(j,\underset{\sim}{L}) \right] \quad .$$

A second canonical transformation leads to the action-angle variables used in the text:

$$q_{\underset{\sim}{k}} = \left(2A_o \, J_{\underset{\sim}{k}} / \omega_k \right)^{\frac{1}{2}} \cos \Theta_{\underset{\sim}{k}} \quad ,$$

$$p_{\underset{\sim}{k}} = -\left(2A_o \, \omega_k \, J_{\underset{\sim}{k}} \right)^{\frac{1}{2}} \sin \Theta_{\underset{\sim}{k}} \quad ,$$

$$Q(j,\underset{\sim}{L}) = \left[2A_o\ J(j,\underset{\sim}{L})/\Omega(j,L)\right]^{\frac{1}{2}} \cos\Theta(j,\underset{\sim}{L}) \quad ,$$

$$P(j,\underset{\sim}{L}) = -\left[2A_o\ \Omega(j,L)\ J(j,\underset{\sim}{L})\right]^{\frac{1}{2}} \sin\Theta(j,\underset{\sim}{L}) \quad . \qquad (A.15)$$

The set of equations, Eq. (35) in the text immediately follow from (A.15).

FIGURE CAPTIONS

1. The modulation of the slope of the mechanically generated surface wave by an internal wave, as measured by Lewis et al. (1974) is compared with the numerical integration of the Hamiltonian equations.

2. The measurements of Joyce (1974) of the resonant internal wave generation by surface waves [⊙] are compared with the "locked phase" approximation (-) and numerical integration of our Hamiltonian equations (---).

3. The energy per mode for surface and internal waves is shown as a function of wavenumber. The equilibrium spectra of Phillips (1966) and Garrett and Munk (1975) with D = 100 m and $\delta\rho/\rho_o = 10^{-3}$ are used.

4. The root mean square amplitudes for resonant triad of Eqs. (49) are shown as a function of time.

5. The root mean square amplitudes for three surface and one internal wave mode [Eqs. (50)] are shown as a function of time.

6. The root mean square amplitudes for three surface and one internal wave mode [Eqs. (51)] are shown as a function of time.

7. E-folding time for growth of an internal wave of wavenumber L due to large amplitude swell is shown. Growth times are shown for the four lowest modes (j=1, 2, 3, 4) and a mixed layer thickness of 100 m. The solid curves correspond to the case that $\delta\rho/\rho_o = 0$, the dashed curves to $\delta\rho/\rho_o = 10^{-3}$.

8. The growth time t_g [Eq. (67)] is shown as a function of mixed layer thickness for $\delta\rho/\rho_o = 0$ and internal wavenumbers (L) of 0.015 m^{-1} and 0.005 m^{-1}.

9. The growth time t_g [Eq. (67)] is shown as a function of

$\delta\rho/\rho_o$ for a mixed layer thickness of 100 m., internal wavenumber 0.01 m^{-1} and modes j = 1, 2, 3.

10. The growth time t_g [Eq. (67)] is shown as a function of wavenumber for a mixed layer thickness of 100 m, $\delta\rho/\rho_o = 0$, and modes j = 1, 2, 3.

11. The growth time t_g [Eq. (67)] is shown as a function of wavenumber for a mixed layer thickness of 100 m., $\delta\rho/\rho_o = 10^{-3}$ and modes j = 1, 2, 3.

12. The root mean square internal mode amplitudes are shown as functions of time using the linear (---) and exact (——) dispersion relations. The internal modes are $L_1 = (10^{-3}m^{-1}$, 83°) and $L_4 = (2\times10^{-3}m^{-1}$, 83°).

13. Contours of equal surface wave height are shown in the two dimensional horizonal plane of the ocean surface at time t = 0 for the four surface modes in Column I of Table II.

14. Contours of equal internal wave height in the two dimensional horizontal plane at time t = 0 for the four internal modes in Column I of Table II as shown.

15. Contours of equal magnitude of surface slope, ie., $|\nabla\zeta|$, in the two dimensional horizontal plane at time t = 0 for the four surface modes in Column I of Table II as shown.

16. Contours of equal internal wave height are shown in the two dimensional horizontal plane of the ocean surface at time $t = 2\times10^4$ sec for the four internal modes in Column I of Table II.

17. Contours of equal magnitude surface wave slope in the two dimensional horizontal plane of the ocean surface at $t = 2\times10^4$ sec for the four surface modes in Column I of Table II as shown.

18. Contours of equal surface wave height are shown in the two dimensional horizontal plane of the ocean surface at time $t = 0$ for the twenty four surface modes in Column II of Table II.

19. Contours of equal internal wave height are shown in the two dimensional horizontal plane of the ocean surface at time $t = 0$ for the ten internal modes in Column II of Table II.

20. Contours of equal magnitude surface wave slope are shown in the two dimensional horizontal plane of the ocean surface at time $t = 10^3$ sec for the twenty four surface modes in Column II of Table II.